Available online at www.sciencedirect.com

ScienceDirect

Geochimica et Cosmochimica Acta 199 (2017) 91–111

Geochimica et Cosmochimica Acta

www.elsevier.com/locate/gca

Molybdenum isotope fractionation in the mantle

Yu-Hsuan Liang [a,b,*], Alex N. Halliday [a], Chris Siebert [c], J. Godfrey Fitton [d], Kevin W. Burton [e], Kuo-Lung Wang [b], Jason Harvey [f]

[a] Department of Earth Sciences, University of Oxford, South Parks Road, Oxford OX1 3AN, UK
[b] Institute of Earth Sciences, Academia Sinica, 128, Sec. 2, Academia Road, Nangang, Taipei 11529, Taiwan
[c] GEOMAR, Helmholtz Center for Ocean Research, Wischhofstrasse 1-3, 24146 Kiel, Germany
[d] School of GeoSciences, University of Edinburgh, Grant Institute, West Mains Road, Edinburgh EH9 3JW, UK
[e] Deparement of Earth Sciences, Durham University, Science Labs, Durham DH1 3LE, UK
[f] School of Earth and Environment, University of Leeds, Leeds LS2 9JT, UK

Received 10 February 2014; accepted in revised form 14 November 2016; available online 20 November 2016

Abstract

We report double-spike molybdenum (Mo) isotope data for forty-two mafic and fifteen ultramafic rocks from diverse locations and compare these with results for five chondrites. The $\delta^{98/95}$Mo values (normalized to NIST SRM 3134) range from -0.59 ± 0.04 to $+0.10 \pm 0.08$‰. The compositions of one carbonaceous (CI) and four ordinary chondrites are relatively uniform (-0.14 ± 0.01‰, 95% ci (confidence interval)) in excellent agreement with previous data. These values are just resolvable from the mean of 10 mid-ocean ridge basalts (MORBs) (0.00 ± 0.02‰, 95% ci). The compositions of 13 mantle-derived ultramafic xenoliths from Kilbourne Hole, Tariat and Vitim are more diverse (-0.39 to -0.07‰) with a mean of -0.22 ± 0.06‰ (95% ci). On this basis, the isotopic composition of the bulk silicate Earth (BSE or Primitive Mantle) is within error identical to chondrites. The mean Mo concentration of the ultramafic xenoliths (0.19 ± 0.07 ppm, 95% ci) is similar in magnitude to that of MORB (0.48 ± 0.13 ppm, 95% ci), providing evidence, either for a more compatible behaviour than previously thought or for selective Mo enrichment of the subcontinental lithospheric mantle. Intraplate and ocean island basalts (OIBs) display significant isotopic variability within a single locality from MORB-like to strongly negative (-0.59 ± 0.04‰). The most extreme values measured are for nephelinites from the Cameroon Line and Trinidade, which also have anomalously high Ce/Pb and low Mo/Ce relative to normal oceanic basalts. $\delta^{98/95}$Mo correlates negatively with Ce/Pb and U/Pb, and positively with Mo/Ce, explicable if a phase such as an oxide or a sulphide liquid selectively retains isotopically heavy Mo in the mantle and fractionates its isotopic composition in low degree partial melts. If residual phases retain Mo during partial melting, it is possible that the [Mo] for the BSE may be misrepresented by values estimated from basalts. This would be consistent with the high Mo concentrations of all the ultramafic xenoliths of 40–400 ppb, similar to or, significantly higher than, current estimates for the BSE (39 ppb). On this basis a revised best estimate of the Mo content in the BSE based on these concentrations would be in the range 113–180 ppb, significantly higher than previously assumed. These values are similar to the levels of depletion in the other refractory moderately siderophile elements W, Ni and Co. A simpler explanation may be that the subcontinental lithospheric mantle has been selectively enriched in Mo leading to the higher concentrations observed. Cryptic melt metasomatism would be difficult to reconcile with the high Mo/Ce of the most LREE depleted xenoliths. Ancient Mo-enriched subducted components would be expected to have heavy $\delta^{98/95}$Mo, which is not observed. The Mo isotope composition of the BSE, cannot be reliably resolved from that of chondrites at this time despite experimental evidence for metal–silicate fractionation. An identical isotopic composition might result from core–mantle differentiation under very high temperatures such as were associated with the Moon-forming Giant Impact, or from the BSE inventory reflecting addition of moderately

* Corresponding author at: Institute of Earth Sciences, Academia Sinica, 128, Sec. 2, Academia Road, Nangang, Taipei 11529, Taiwan. Fax: +886 2 27839871.
E-mail address: yuhsuanl@earth.sinica.edu.tw (Y.-H. Liang).

http://dx.doi.org/10.1016/j.gca.2016.11.023
0016-7037/

siderophile elements from an oxidised Moon-forming impactor (O'Neill, 1991). However, the latter would be inconsistent with the non-chondritic radiogenic W isotopic composition of the BSE. Based on mantle fertility arguments, Mo in the BSE could even be lighter (lower $^{98/95}$Mo) than that in chondrites, which might be explained by loss of S rich liquids from the BSE during core formation (Wade et al., 2012). Such a late removal model is no longer required to explain the Mo concentration of the BSE if its abundance is in fact much higher, and similar to the values for ultramafic xenoliths.

Keywords: Molybdenum; Isotope fractionation; Bulk silicate Earth; Chondrites; Mantle derived rocks

1. INTRODUCTION

Molybdenum (Mo) is an economically important element, the geochemistry of which is interesting from a variety of viewpoints. It has long been considered the most strongly depleted of the moderately siderophile, refractory elements in the bulk silicate Earth (BSE or primitive mantle), showing an apparent well-defined ~70-fold reduction relative to refractory lithophile elements as a result of core formation (Palme and O'Neill, 2007). This has led to very specific models about its removal in S rich liquids during late stage core formation (Wade et al., 2012). Molybdenum is considered to be incompatible during mantle melting, with a bulk distribution coefficient comparable to that of light rare earths (Sims et al., 1990). On this basis, about 10% of the Mo in the BSE is thought to reside in the continental crust.

During core–mantle differentiation, differences in bonding between metallic or sulphur-rich liquids and silicate or silicate liquids are likely to generate small but potentially measurable isotopic effects (Georg et al., 2007; Hin et al., 2013). For the Mo isotopic system, only a few such data are available. Experimental and meteorite data published by Hin et al. (2013) and Burkhardt et al. (2014) provide evidence that the fractionation of Mo isotopes during core–mantle differentiation might depend on the temperature of metal–silicate equilibration. Most other published meteorite Mo isotope data are normalized to an internal isotope ratio to demonstrate small nucleosynthetic differences (Burkhardt et al., 2011 and references therein). In this paper we provide the first comprehensive dataset for the Mo isotopic compositions of rocks derived from the Earth's mantle.

Published data on terrestrial rocks from high temperature settings currently are limited. Significant Mo isotope fractionation in molybdenites from mineral deposits is reported by Hannah et al. (2007) and Mathur et al. (2010) and can be large, possibly reflecting fractionation between different mineral phases during ore-forming processes (Mathur et al., 2010). More recently, Greber et al. (2014) presented Mo isotopic data for molybdenite samples from the porphyry-type Questa deposit, and suggest that the first step of isotopic fractionation is during progressive fractional crystallization in subvolcanic magma reservoirs when heavy Mo isotopes are preferentially retained in the melt with lighter isotopes more strongly incorporated into crystallizing phases. This is repeated as molybdenites crystallize from hydrothermal fluids, leading to a progressive change in the bulk Mo isotope composition. Voegelin et al. (2014) also demonstrated fractionation of Mo isotopes by the mafic hydrous minerals hornblende and biotite during magmatic differentiation in an arc system at Kos. Yang et al. (2015) found no Mo isotopic fractionation from basalt to rhyolite, in the absence of hydrous minerals, at Hekla volcano (Iceland). Most recently, Greber et al. (2015) published Mo isotopic and concentration data for komatiites, refining the Mo concentration of the bulk silicate Earth (BSE) as 23 ± 7 ng/g with an isotopic composition ($\delta^{98/95}$Mo) of -0.21 ± 0.06‰ (re-normalised to the value of NIST SRM 3134 for comparison with this study).

Despite these studies there is still no well-defined Mo isotope composition for the present day oceanic crust and pristine ultramafic xenolith samples of the upper mantle. In this study we report new data for bulk meteorites (carbonaceous and ordinary chondrite), and mafic and ultramafic rocks from a variety of such settings to determine the processes of fractionation associated with partial melting and the Mo isotope composition of the mantle (and hence the BSE).

2. SAMPLING

Well characterised samples were selected from a variety of geological settings and include 42 mafic and 15 ultramafic rocks (as listed in Table 1). Four of these are mantle-derived USGS standards included to provide quality control. BCR-2 and BHVO-2 are basalt standards, and DTS-1 and PCC-1 are ultramafic rocks (Table 1). Five meteorites are also included, comprising one carbonaceous chondrite and four ordinary chondrites, in order to compare with terrestrial samples and provide information on fractionation during terrestrial core formation.

The ultramafic xenoliths studied here are thought to be direct samples of the upper mantle from three localities. Three lherzolites and harzburgites have been analysed from Kilbourne Hole (Rio Grande Rift) and are well characterised in terms of their mineral, major and trace element composition (Harvey et al., 2011, 2012). A further ten ultramafic xenoliths are from Tariat (Mongolia) and Vitim (Siberia). The ultramafic xenolith suites of these last two localities have also been well studied (Ionov et al., 2005; Ionov, 2007; Wang et al., 2013 and references therein). The xenoliths are fresh spinel lherzolites, and deformation or recrystallization textures are rare (Wang et al., 2013). Tariat xenoliths are exhumed by Quaternary magmatism (Harris et al., 2010), and Vitim xenoliths are from a Miocene picritic tuff (Ionov, 2004).

USGS ultramafic rock standard PCC-1 is a peridotite from the Cazadero ultramafic massif located in California

Table 1
Molybdenum concentration and isotope compositions for all of the samples in this study.

Sample		Locality	n[a]	Mo (ppm)	$\delta^{98/95}Mo_{SRM3134}$[b] (‰)
Carbonaceous chondrite					
Orgueil	CI		4	0.95 ± 0.05	−0.12 ± 0.11
Ordinary chondrite					
Bremervörde	H/L3		1	1.01 ± 0.05	−0.15 ± 0.08
Barratta	L4		4	0.79 ± 0.04	−0.14 ± 0.06
Bruderheim	L6		1	0.78 ± 0.04	−0.14 ± 0.08
Parnallee	LL3		5	0.63 ± 0.03	−0.13 ± 0.05
Ultramafic rocks					
DTS-1	Dunite	Twin Sisters, Washington	3	0.03 ± 0.002	−0.14 ± 0.08
PCC-1	Peridotite	Cazadero Complex, California	3	0.02 ± 0.001	−0.14 ± 0.06
KH96-8	Lherzolite	Kilbourne Hole	2	0.09 ± 0.005	−0.39 ± 0.09
KH03-10	Lherzolite	Kilbourne Hole	1	0.05 ± 0.003	−0.30 ± 0.07
KH03-16	Harzburgite	Kilbourne Hole	1	0.04 ± 0.002	−0.07 ± 0.07
Mean of Kilbourne hole					*−0.25 ± 0.34*
ST0802	Spinel lherzolite	Tariat, Mongolia	1	0.29 ± 0.01	−0.17 ± 0.06
ST0803	Spinel lherzolite	Tariat, Mongolia	1	0.12 ± 0.01	−0.30 ± 0.06
ST0804	Spinel lherzolite	Tariat, Mongolia	1	0.29 ± 0.01	−0.10 ± 0.06
ST0805	Spinel lherzolite	Tariat, Mongolia	1	0.21 ± 0.01	−0.23 ± 0.07
ST0807	Spinel lherzolite	Tariat, Mongolia	1	0.13 ± 0.01	−0.32 ± 0.07
ST0809	Spinel lherzolite	Tariat, Mongolia	2	0.40 ± 0.02	−0.14 ± 0.07
Mean of Tariat, Mongolia					*−0.21 ± 0.08*
PQ0902	Spinel lherzolite	Vitim, Siberia	1	0.13 ± 0.01	−0.17 ± 0.06
PQ0903	Spinel lherzolite	Vitim, Siberia	2	0.40 ± 0.02	−0.16 ± 0.06
PQ0910	Spinel lherzolite	Vitim, Siberia	1	0.15 ± 0.01	−0.22 ± 0.06
L-3-2	Spinel lherzolite	Vitim, Siberia	1	0.13 ± 0.01	−0.24 ± 0.06
Mean of Vitim, Siberia					*−0.20 ± 0.05*
Mean of ultramafic rocks				*0.17 ± 0.07*	*−0.19 ± 0.06*
Mean of ultramafic xenoliths				*0.19 ± 0.07*	*−0.22 ± 0.06*
Submarine mid-ocean ridge basalts (MORB)					
MD34 D6	Basalt (E-type MORB)	Southwest Indian Ridge	1	0.62 ± 0.03	0.05 ± 0.08
45N	Basalt (E-type MORB)	Mid-Atlantic Ridge	1	0.43 ± 0.02	0.03 ± 0.07
ALV 518 3-1	Basalt (E-type MORB)	Mid-Atlantic Ridge	2	0.42 ± 0.02	0.02 ± 0.09
ALV 518 3-2	Basalt (E-type MORB)	Mid-Atlantic Ridge	2	0.43 ± 0.02	−0.05 ± 0.09
ARP 1974 12-19	Basalt (N-type MORB)	Mid-Atlantic Ridge	2	0.32 ± 0.02	0.00 ± 0.07
CY82 18-01	Basalt (N-type MORB)	East Pacific Rise	1	0.46 ± 0.02	−0.04 ± 0.09
DR 7-1	Basalt (E-type MORB)	East Pacific Rise	2	0.93 ± 0.05	−0.02 ± 0.09
R82-1	Basalt (N-type MORB)	East Pacific Rise	2	0.23 ± 0.01	0.03 ± 0.06
R93-7	Basalt (E-type MORB)	East Pacific Rise	2	0.58 ± 0.03	−0.01 ± 0.08
Searise 2 DR07	Basalt (N-type MORB)	East Pacific Rise	1	0.40 ± 0.02	0.04 ± 0.09
Mean of MORBs				*0.48 ± 0.13*	*0.00 ± 0.02*

(*continued on next page*)

Table 1 (*continued*)

Sample		Locality	n[a]	Mo (ppm)	$\delta^{98/95}Mo_{SRM3134}$[b] (‰)
Plume-ridge interacting basalts					
CX19	Basalt	Iceland	2	0.56 ± 0.03	−0.14 ± 0.06
GS18	Basalt	Iceland	3	0.25 ± 0.01	−0.34 ± 0.06
SNB19	Basalt	Iceland	2	1.19 ± 0.06	−0.18 ± 0.06
SNB40	Basalt	Iceland	2	1.09 ± 0.05	−0.22 ± 0.12
ST38	Basalt	Iceland	3	0.48 ± 0.02	−0.41 ± 0.12
Mean of plume-ridge interacting basalts				*0.72 ± 0.34*	*−0.26 ± 0.12*
Ocean island basalts (OIB) and continental intraplate basalts					
BCR-2	Basalt	Columbia River, Oregon	3	236 ± 6	−0.03 ± 0.04
BHVO-2	Basalt	Halemaumau, Hawaii	22	3.48 ± 0.17	−0.03 ± 0.04
AZF1	Alkali basalt	Azores	3	2.76 ± 0.14	−0.19 ± 0.04
AZFY3	Alkali basalt	Azores	1	2.18 ± 0.11	−0.05 ± 0.07
AZP5	Transitional basalt	Azores	3	1.14 ± 0.06	0.01 ± 0.12
AZP6	Alkali basalt	Azores	3	3.10 ± 0.15	0.05 ± 0.04
C1	Alkali basalt	Cameroon Line (Mt Cameroon)	3	3.52 ± 0.18	−0.17 ± 0.08
C20	Nephelinite	Cameroon Line (Etinde)	3	1.65 ± 0.08	−0.59 ± 0.04
C22	Nephelinite	Cameroon Line (Etinde)	3	4.12 ± 0.21	−0.15 ± 0.10
C25	Basanite	Cameroon Line (Mt Cameroon)	3	3.39 ± 0.17	−0.14 ± 0.06
C30	Basanite	Cameroon Line (Mt Cameroon)	3	2.07 ± 0.10	−0.14 ± 0.08
C51	Alkali basalt	Cameroon Line (Manengouba)	3	2.10 ± 0.11	−0.20 ± 0.08
C72	Alkali basalt	Cameroon Line (Manengouba)	3	2.03 ± 0.10	−0.12 ± 0.04
C128	Nephelinite	Cameroon Line (Etinde)	3	4.17 ± 0.21	−0.21 ± 0.11
C150	Olivine melanephelinite	Cameroon Line (Etinde)	3	2.57 ± 0.13	−0.43 ± 0.11
C152	Hauyne nephelinite	Cameroon Line (Etinde)	3	16.1 ± 0.8	−0.12 ± 0.05
C154	Nosean leucite nephelinite	Cameroon Line (Etinde)	3	3.91 ± 0.20	−0.07 ± 0.07
C192	Basanite	Cameroon Line (Mt Cameroon)	3	2.86 ± 0.14	−0.07 ± 0.05
FP23	Alkali basalt	Cameroon Line (Bioko)	3	1.81 ± 0.09	−0.12 ± 0.13
PL02 25-1	Alkali basalt	Galapagos	3	1.28 ± 0.06	−0.09 ± 0.04
PL02 30-1	Tholeiite	Galapagos	3	0.69 ± 0.03	0.01 ± 0.07
D4-6	Alkali basalt	Loihi	2	0.83 ± 0.04	−0.07 ± 0.15
D5-1	Alkali basalt	Loihi	2	0.91 ± 0.05	−0.03 ± 0.12
M40	Alkali basalt	Madeira	2	1.27 ± 0.06	−0.17 ± 0.15
TD2	Tephrite	Trinidade	2	0.91 ± 0.05	0.10 ± 0.08
TD4	Nephelinite	Trinidade	2	3.82 ± 0.19	−0.23 ± 0.14
TD5	Nephelinite	Trinidade	2	3.19 ± 0.16	−0.36 ± 0.08
Mean of OIBs				*2.90 ± 1.20*	*−0.14 ± 0.06*

[a] Number of duplicates for the same sample.

[b] If only one aliquot successfully analysed for the sample, so the errors are given as 2 standard deviation of standard measurements in each measuring session. If only two aliquots successfully analysed for the sample, the errors are given 2 standard deviations for all duplicates of each sample, or 2 standard deviation of standard measurements in each measuring session, whichever is larger. If more than two aliquots successfully analysed for the sample, the errors are given as 95% confidence intervals of all duplicates of the sample.

and DTS-1 is a dunite from Twin Sisters area of Washington State (Flanagan, 1967). The Twin Sisters dunite has large olivine crystals which were subsequently partially recrystallized and/or mylonitized in the upper mantle, as well as chromite pods and lenses (Onyeagocha, 1978). These two standard ultramafic rock samples may not be pristine upper mantle lithologies.

Mid-ocean ridge basalts (MORBs) are thought to be melts of upper mantle sources carrying Nd and Sr radiogenic isotopic compositions that reflect a time-integrated history of melt depletion. The data set here uses 10 optically clear submarine MORB glasses spanning differing degrees of partial melting and mainly from the Mid-Atlantic Ridge, Southwest Indian Ridge, and East Pacific Rise (Niu and Batiza, 1997; Schiano et al., 1997; Gannoun et al., 2007).

In contrast to MORBs, the relatively incompatible element enriched sources of OIBs have been ascribed to the long-term cycling of sub-continental lithospheric mantle material (Galer and O'Nions, 1986), the addition of subducted oceanic crust to the source (Hofmann and White, 1982) and intramantle melt enrichment (Halliday et al., 1992, 1995). Therefore, the Mo isotopic characteristics of OIBs and MORBs might reflect that of distinct mantle reservoirs. Twenty-five OIB samples from both the Atlantic and Pacific Oceans have been analysed for this study. Samples from the Atlantic Ocean include the Azores, the Cameroon Line, Madeira, and Trinidade, which have been studied for their major, trace element and Nd, Sr, and Pb radiogenic isotopic compositions (Halliday et al., 1990, 1995; Yi et al., 1995). Four samples from the Pacific Ocean are from the Galapagos Islands and Loihi Seamount. These samples are submarine lavas and are also characterised for major and trace elements (Yi et al., 2000).

Iceland is thought to represent the surface expression of a mantle plume intersecting a mid-ocean ridge and offers an unusual opportunity to investigate large-degree partial melting (Schilling et al., 1982). The Mid-Atlantic Ridge on Iceland is represented by a southwest- to north-striking zone of late Quaternary volcanism (less than 0.7 Ma). These neovolcanic zones are enclosed by Pliocene–Pleistocene formations to the east and Tertiary lava piles to the west (e.g. Hardarson and Fitton, 1997). In order to compare volcanic rocks of different ages, we chose two Quaternary samples from Snaefellsnes, which is an area of isolated off-axis volcanism, and we also analysed three Tertiary basalts (between 12.4 and 5.3 Ma) sampled from eastern and northern Iceland (Hardarson and Fitton, 1997). Tertiary and Pliocene–Pleistocene basalt lavas are remarkably uniform in chemical and isotopic composition compared with lavas in the rift zones (Schilling et al., 1982). However, Hardarson and Fitton (1997) have shown that large flows that originated within the axial zone and spread far enough to become preserved in the accessible part of the future off-axis lava pile are very homogeneous in composition and comparable to those forming the Tertiary lava successions.

The carbonaceous and ordinary chondrites were chosen because they are samples of primitive materials that are thought to be representative of portions of the disk from which the protoplanets accreted that ultimately built the Earth. They have concentrations of Mo thought to be similar to the bulk Earth. The specific meteorites have been selected because they have small or negligible nucleosynthetic differences relative to terrestrial Mo. Before determining the mass-dependent isotope variation in meteorites, the nucleosynthetic mass-independent isotope composition needs to be known. Several previous studies (Dauphas et al., 2002; Yin et al., 2002; Becker and Walker, 2003) were not able to resolve Mo isotopic differences between terrestrial samples and ordinary chondrites. Burkhardt et al. (2011) reported mass-independent Mo isotopic anomalies for ordinary chondrites that were generally smaller than (or equal to) their analytical uncertainties. The mass-dependent Mo isotope fractionation of the chondritic reservoir is also quite limited (Burkhardt et al., 2014). Thus ordinary chondrites would be straightforward material to represent Earth-like material for our purposes.

The composition of bulk Ivuna-type carbonaceous chondrites (CI) is viewed as a measure of average Solar-System abundances and is used as a reference planetary composition, while other classes of carbonaceous chondrites (e.g. CV and CM) display more significant nucleosynthetic differences relative to Earth (Burkhardt et al., 2011). Therefore, one CI chondrite (Orgueil) is also included in the sample set.

3. METHODS

The analytical methods in this study principally follow the techniques described in Siebert et al. (2001). Mid-ocean ridge basalts were handpicked under the binocular microscope and then digested as small pieces of fresh glass. Ultramafic xenoliths and OIBs were carefully cleaned and crushed with an agate or tungsten carbide ball mill, while all of the chondrites were crushed with an aluminium oxide mortar.

For correction of instrumental and laboratory mass fractionation, all samples were spiked with a double isotope tracer (^{100}Mo, ^{97}Mo) prior to digestion. All of the mafic rocks were dissolved with a mixture of HF and HNO_3 in sealed Teflon vials on a hotplate at 140 °C for at least 3 days. Ultramafic rocks and meteorites that might contain refractory minerals were digested using pressurised PTFE Teflon bombs (Prytulak et al., 2011). In order to make certain that all refractory components were dissolved, this bomb digestion technique was repeated up to three times for some samples. The samples were then taken up in 5 M HCl for chemical separation. Samples were loaded on 2 ml of Biorad AG1-X8 anion exchange resin rinsed with 5 M HCl to remove most of the major and trace elements and then eluted with 1 M HCl. The eluents were dried and then passed through 2 ml of Biorad AG50W-X8 cation resin in 0.5 M HCl to remove Fe. Total procedural blanks were <3 ng of Mo for basalts samples and <1 ng of Mo for ultramafic samples. The sample amount was normally between 50 and 300 mg but was increased up to 1 g when processing low Mo abundance samples, such as some ultramafic xenoliths, to keep the blank contribution negligible. More details about sample digestion, chemical separation of Mo, and Mo isotope measurements are given in the Appendix.

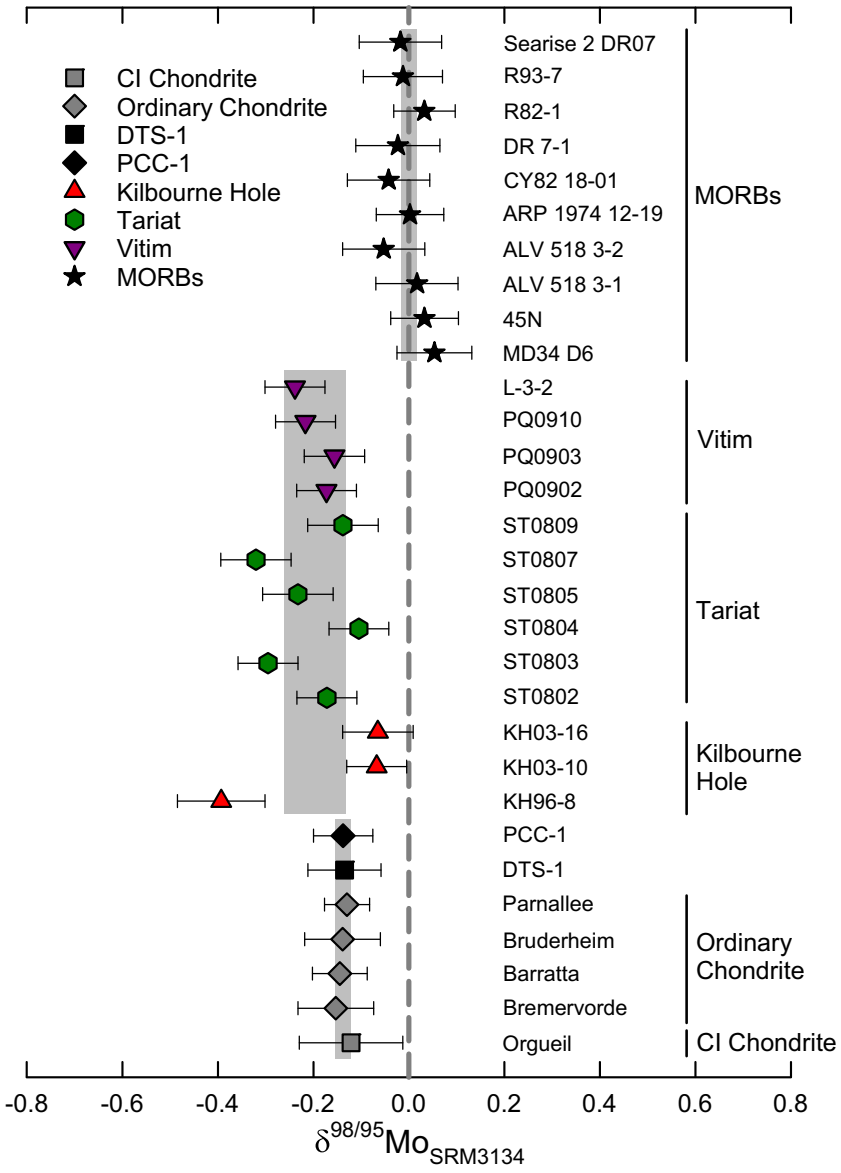

Fig. 1. The Mo isotope compositions for all of the chondrite, ultramafic and mid-ocean ridge basalt samples in this study. The grey bars show the average of different rock types. The long-term external standard reproducibility of $^{98}Mo/^{95}Mo$ is ±0.09‰.

Molybdenum isotopic composition measurements were made on a Nu Instruments® MC-ICPMS with DSN-100 Desolvation Nebulizer System at the Department of Earth Sciences, University of Oxford. Both Alfa Aesar Mo plasma standard solution, Specpure® #38791 (lot No. 011895D) and NIST SRM 3134 were used as laboratory and measurement standards. The samples and standard solutions always had the same concentration during the measurement. The concentrations of Mo in the measurement solutions were between 15 and 30 ppb, while the measurement ion beam intensities were usually between 80 and 130 V per ppm, as measured using 10^{11} Ω resistors. Each measurement was the average of 2 blocks of 40 cycles, each with an integration time of 5 s. The Mo isotopes that have isobaric interferences with Zr isotopes were not used in the calculation. Iron argides might also provide potential interferences, but tests were always run before measurements to make sure they were all lower than the instrument background. We also monitored ^{99}Ru in order to confirm that there was no Ru interference higher than the instrument background level. All Mo isotopic variations are represented by the delta notation as the deviation in parts per thousand (‰):

$$\delta^{98/95}\mathrm{Mo} = \left(\frac{(^{98}\mathrm{Mo}/^{95}\mathrm{Mo})_{\mathrm{sample}}}{(^{98}\mathrm{Mo}/^{95}\mathrm{Mo})_{\mathrm{standard}}} - 1 \right) \times 1000$$

For this study, each duplicate analysis consists of a repeat of the entire procedure from the same crushed rock sample. Each batch of sample processing and measuring always included at least one aliquot of BHVO-2, sometimes together with BCR-2, as well as samples from different

groups and localities. For example, OIB from various locations were always processed together with some MORBs or ultramafic rocks. Therefore, consistent differences between OIB, MORB and ultramafic rocks have been demonstrated both within and between analytical sessions.

The external standard reproducibility of the $\delta^{98/95}$Mo values over the time period of sample analysis is ±0.09‰ (2SD). The long-term reproducibility on $\delta^{98/95}$Mo values for BCR-2 and BHVO-2 are both ±0.04‰ (Table 1).

Greber et al. (2012) published Mo concentrations and $\delta^{98/95}$Mo for several NIST reference materials and suggested SRM 3134 as an interlaboratory reference standard for Mo isotope composition. Based on our own double-spike calibration and measurements, the Mo isotope value of the Alfa Aesar standard solution used in this study is offset from NIST SRM 3134 by a $\delta^{98/95}Mo_{SRM\ 3134}$ value of -0.15 ± 0.03‰ (2SD). To facilitate interlaboratory comparisons all data reported here have been normalized to the NIST SRM3134 value.

4. RESULTS

The Mo isotopic compositions and concentration for all samples are shown in Table 1, Figs. 1 and 2 (expressed relative to the composition of the NIST SRM3134 standard). The errors in Table 1, text, and figures are 95% confidence intervals of sample reproducibility. If only one aliquot of the sample was measured the error is given as 2 standard deviations of the Alfa standard reproducibility during the measurement at the same period of time. If only two aliquots of the sample were measured the error is given as 2 standard deviations of the standard reproducibility during the measurement at the same period of time, or 2 standard deviations of sample reproducibility, whichever is larger.

Both BCR-2 and BHVO-2 show very good reproducibility and identical average $\delta^{98/95}$Mo values of -0.03 ± 0.04‰. These two well-characterised basaltic standards are suitable for representing the data quality, but data for BCR-2 and BHVO-2 should be interpreted with caution geologically speaking because of the likelihood of crustal contamination in the former (as demonstrated by the extremely high Mo content) and diverse Mo contents reported in different batches for the latter. The ultramafic rock standards, DTS-1 and PCC-1, have low Mo contents (0.02–0.03 ppm), and the average $\delta^{98/95}$Mo is -0.14 ± 0.08‰ for DTS-1 and -0.14 ± 0.06‰ for PCC-1. Although the USGS standards may have Mo isotopic compositions sim-

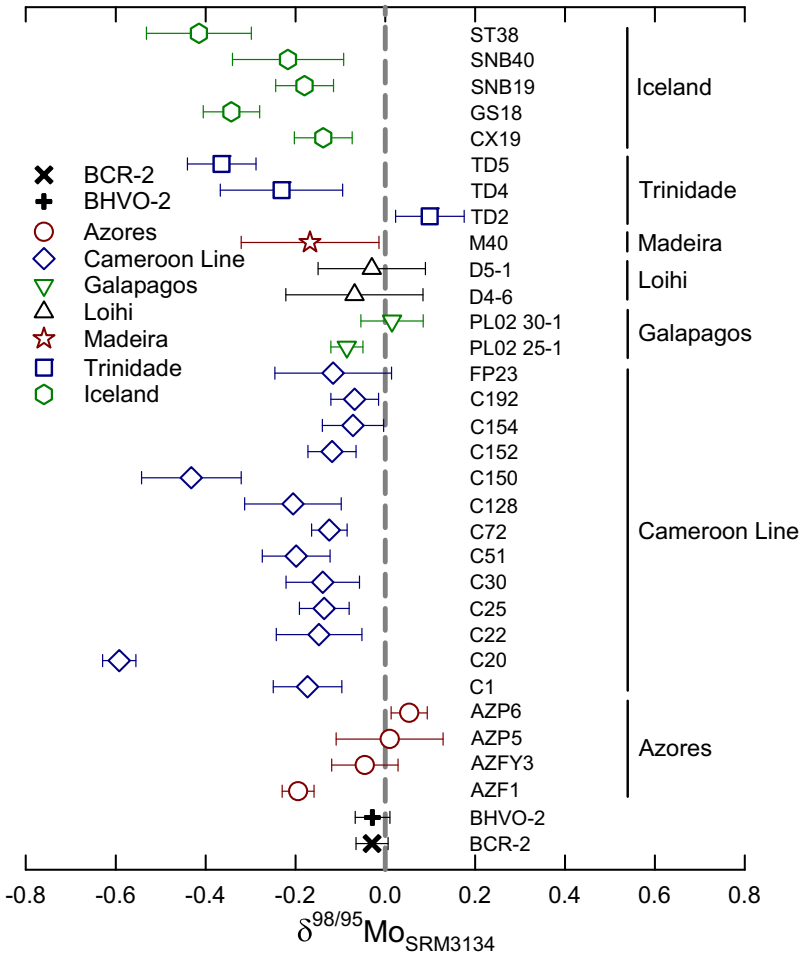

Fig. 2. The Mo isotope compositions for all of the plume-ridge interacting basalt, ocean island basalts and continental intraplate basalt samples in this study. The long-term external standard reproducibility of $^{98}Mo/^{95}Mo$ is ±0.09‰.

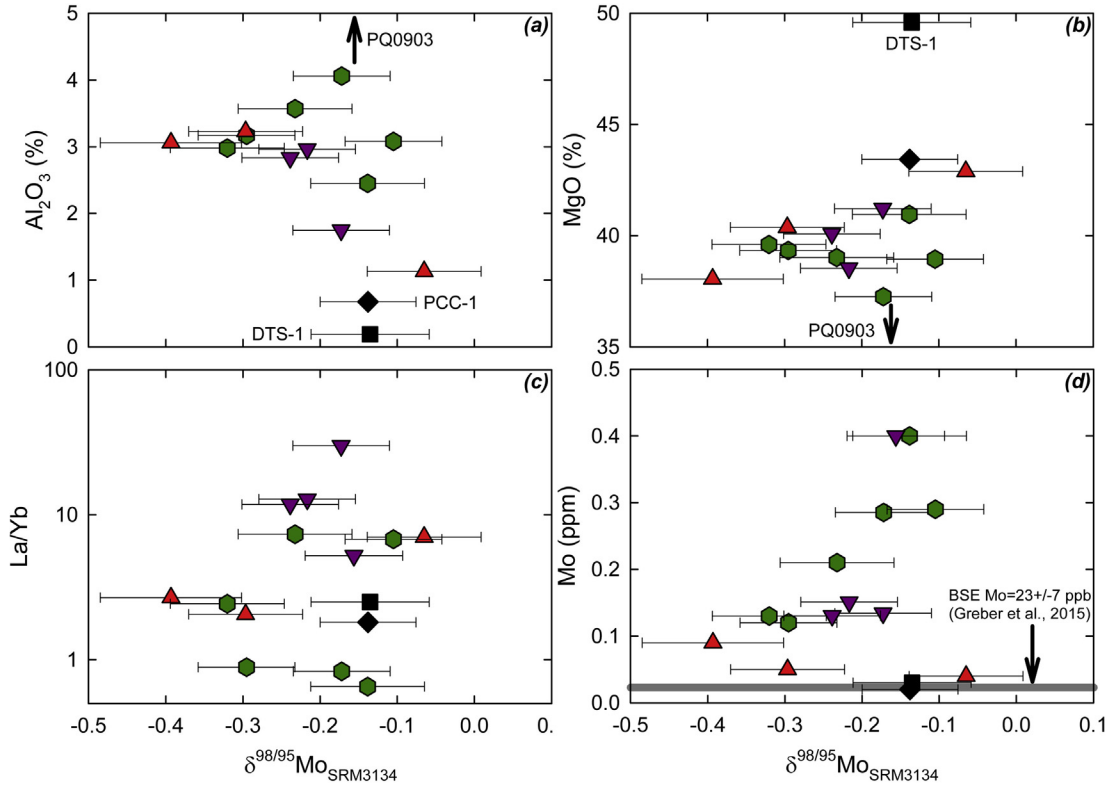

Fig. 3. Bulk (a) Al_2O_3 contents, (b) MgO contents, (c) La/Yb, and (d) Mo contents plotted against $\delta^{98/95}$Mo values for ultramafic rocks. Data from Table 1 and Appendix Table A1. Symbols as in Fig. 1.

ilar to other samples, we do not use these mass-produced reference materials in our discussion.

The Mo contents of chondrites vary by a factor of 2, but all the investigated chondrites have uniform $\delta^{98/95}Mo_{SRM3134}$ of between -0.15 ± 0.08‰ and -0.12 ± 0.11‰. These results have been corrected for nucleosynthetic anomalies reported by Burkhardt et al. (2011).

The ultramafic xenoliths from Kilbourne Hole have slightly higher Mo contents (0.04–0.09 ppm) than those of DTS-1 and PCC-1; the isotope compositions vary between −0.39 and −0.07‰. The ultramafic xenoliths sampled from Tariat and Vitim have still higher Mo contents (0.12–0.40 ppm), but the $\delta^{98/95}$Mo values define a similar range (from −0.32 to −0.10‰) to those at Kilbourne Hole. Peridotite xenoliths can suffer from supergene weathering which has the potential to oxidise and mobilise certain elements (S, Os, maybe even Se) when they are exposed to surface/meteoric water. If Mo behaves in this way then estimates for concentrations are likely to be minima. However, there is no evidence for such alteration in these samples. The $\delta^{98/95}$Mo values bear no obvious relationship with ultramafic rock type (Table 1). Note that an earlier report by Liang et al. (2013) claimed that there are both heavier Mo isotopic compositions and still higher Mo concentrations in ultramafic xenoliths. These samples from Lashaine (Tanzania) were provided in powdered form and there is evidence that the data may have been affected by contamination during crushing. So these data are not reported here.

The $\delta^{98/95}$Mo of all MORBs is relatively uniform ranging between 0.05 and −0.05‰ with a mean of 0.00 ± 0.02‰ (95% ci). In contrast to MORB, the results for OIBs display a significant range from −0.59‰ to +0.10‰. Large differences are even found in samples from the same location (Table 1, Fig. 2). The Mo content in these OIBs shows a large spread (0.25–16 ppm) while MORB ranges from 0.23 to 0.93 ppm.

5. DISCUSSION

5.1. Isotopic homogeneity of ordinary chondrite and CI carbonaceous chondrite

Different groups of ordinary chondrites (from H to LL) were included in the sample set. Siderophile element abundances should decrease and oxidation state should increase through the sequence H–L–LL (Krot et al., 2007), so Mo concentration varies in a manner consistent with its siderophile affinity. The Mo isotope composition of ordinary chondrites appears unaffected by the oxidation state of the parent asteroids and there is no evidence that differing proportions of metallic iron fractionate Mo isotopes.

The Mo isotopic composition of the analysed CI chondrite ($\delta^{98/95}Mo_{SRM3134} = -0.12 \pm 0.11$‰) is also identical to the values observed in ordinary chondrites (−0.15 to −0.13‰). Generally, CI chondrites are thought to be the most primitive meteorites compositionally and provide the best match to the solar photosphere, although they also contain some secondary mineral phases that provide a record of extensive and multistage aqueous alteration on their parent body (Endress et al., 1996 and references

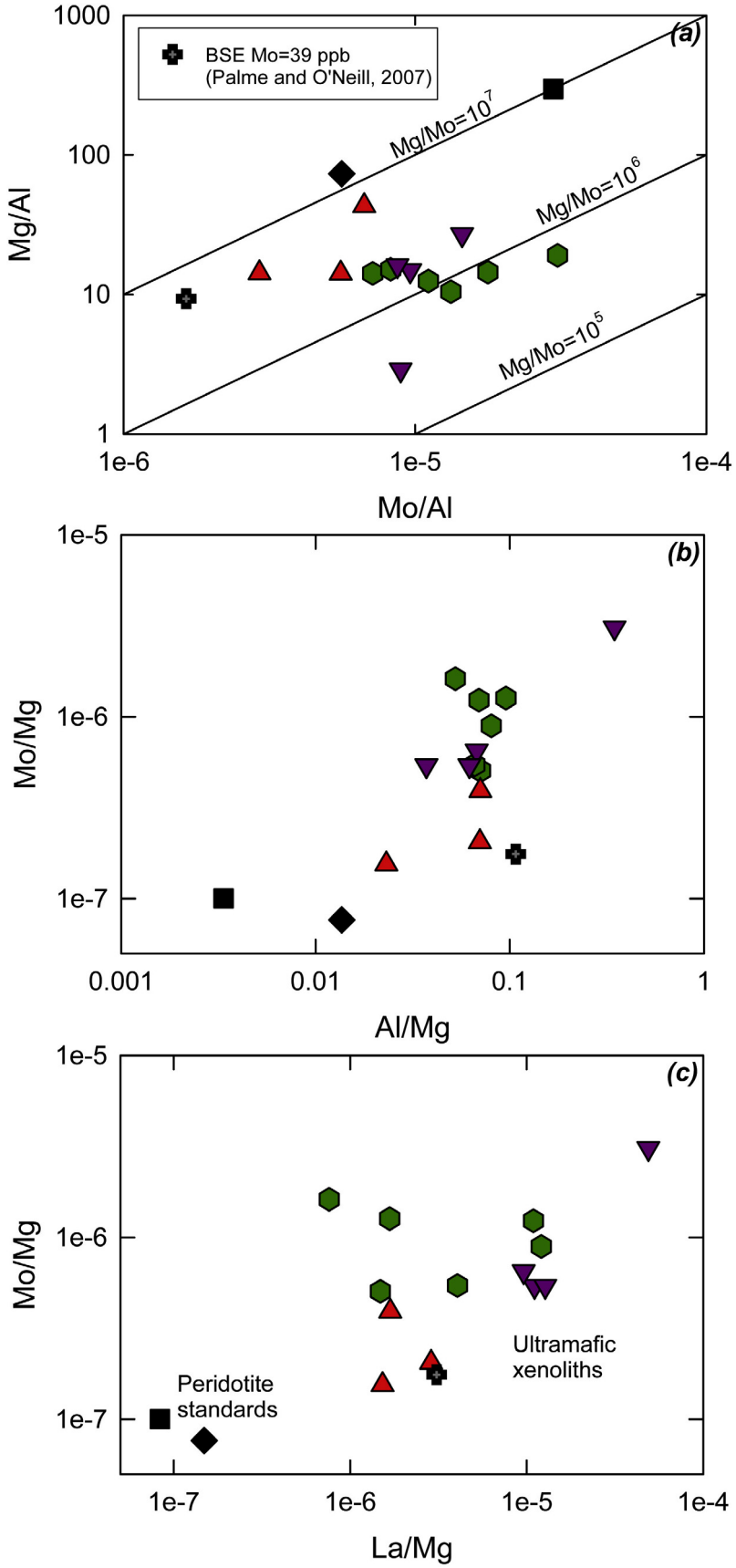

Fig. 4. (a) Mg/Al against Mo/Al, (b) Mo/Mg against Al/Mg, and (c) Mo/Mg against La/Mg for ultramafic rocks. Data from Table 1 and Appendix Table A1. Symbols as in Fig. 1.

therein). However, the results for the CI chondrite indicate that these processes do not fractionate Mo isotopes significantly (i.e. within the analytical error), and lead to identical values for CI and ordinary chondrites. The mean of all 5 chondrites is -0.14 ± 0.02‰ (95% ci). Similar results are reported by Burkhardt et al. (2014) who obtain indistinguishable $\delta^{98/95}Mo_{SRM\ 3134}$ values of ordinary and carbonaceous chondrite with the exception of CM and CK which have been deliberately avoided in our study to limit any complications associated with resolving nucleosynthetic and mass dependent variations (Burkhardt et al., 2011, 2014). Their equivalent data average -0.16 ± 0.02‰, which is in excellent agreement with our results.

5.2. Ultramafic xenoliths and the sub-continental lithospheric mantle

The average $\delta^{98/95}$Mo of the ultramafic rocks is -0.19 ± 0.06‰ (95% ci), or -0.22 ± 0.06‰ (95% ci) if one excludes the USGS standards. Both values overlap with the average chondrite isotopic composition of -0.14 ± 0.02‰, the literature chondritic value (Burkhardt et al., 2014) and the mean value of investigated komatiites (Greber et al., 2015). If this is representative of the whole mantle there is limited or no isotopic fractionation during core formation (cf. Burkhardt et al. (2014)).

The concentrations of Al_2O_3 and MgO are commonly considered to vary positively and negatively respectively with fertility of the upper mantle. The Mo isotopic compositions show no correlation with Al_2O_3 (Fig. 3a) but a hint of positive correlation with MgO (Fig. 3b). One of the samples from Vitim has extremely high Al_2O_3 and low MgO. Since it has an Al_2O_3 abundance (8.5%) far in excess of modelled fertile upper mantle (Walter, 2003), this might indicate this ultramafic sample is a product of refertilisation (Soustelle et al., 2009; Harvey et al., 2012). Therefore, this sample is excluded from further consideration here. The two USGS standards plot with anomalously low and high Al_2O_3 and MgO respectively (Fig. 3a and b), which might reflect cumulate origins. Again, these are excluded from further consideration here because of their uncertain origin.

The $\delta^{98/95}$Mo values do not show any correlation with La/Yb (Fig. 3c) that might otherwise reflect the effects of cryptic metasomatic enrichment by small degree partial melts. In Fig. 3d the isotopic compositions are compared with Mo concentrations. The Tariat and Vitim samples display an interesting common curved trend whereas the three Kilbourne Hole xenoliths plot off this trend, and if anything display a negative correlation between the two parameters (Fig. 3d). The suggestion that more depleted compositions (from a major element perspective) are related by melt extraction (Dawson, 2002) to heavier residual $\delta^{98/95}$Mo (Fig. 3b), which in turn is related to generally higher Mo concentrations for Vitim and Tariat (Fig. 3d), might seem hard to reconcile with the conventional view that Mo is an incompatible element. Associations of incompatible trace element enrichment with major element melt depletion have previously been reported for ultramafic xenoliths (Lee et al., 1996; Ionov et al., 2002) and are thought to reflect metasomatism by low degree partial melts permeating highly depleted cratonic sub continental lithospheric mantle (Navon and Stolper, 1987; Bodinier et al., 1990; Vasseur et al., 1991). However, this interpretation is not supported by the scatter in Fig. 3c.

As shown in Fig. 3d, all of these xenoliths have Mo concentrations that are higher than the BSE value of 23 ± 7 ng/g recommended by Greber et al. (2015) based on komatiite data. They are also all higher or in one instance about equal to the BSE value of 39 ng/g recommended by Palme and O'Neill (2007). Either the subcontinental lithospheric mantle as sampled by the xenoliths is especially Mo enriched, or these BSE values are incorrect. There is no evidence of a simple single fractionating process or component that is responsible for the Mo enrichment of the lithospheric mantle.

In Fig. 4 the degree of Mo enrichment as a function of fertility and enrichment is explored further with element ratio plots. Although there is no relationship between Mo/Al and Mg/Al (Fig. 4a) there is a correlation between Mo/Mg and Al/Mg (Fig. 4b) consistent with Mo being a slightly incompatible element whose abundance is controlled by the overall level of melt depletion and not cryptic metasomatism. This is endorsed by the lack of correlation between Mo/Mg and La/Mg (Fig. 4c).

The degree of incompatibility of Mo in silicate melting and differentiation has been the subject of some uncertainty. Initially it was shown that Mo/Pr is approximately uniform in MORBs and normal OIBs (Hofmann et al., 1986; Newsom et al., 1986). It was then demonstrated that Mo may be more like Ce in its incompatibility and the Mo/Ce values in MORB have been used for estimating the Mo abundance of the primitive mantle (Sims et al., 1990). The Mo/Ce vlaue is highly variable from 0.023 to 0.92 in the xenoliths (Fig. 5), ranging *well* above the BSE value of 0.022 (Palme and O'Neill, 2007) and 0.013 as calculated from Greber et al. (2015). There is no positive relationship between Mo/Ce and LREE enrichment (La/Yb, Fig. 5) as might be expected if the Mo over enrichment were caused by "normal" melt metasomatism. The data do lie close to

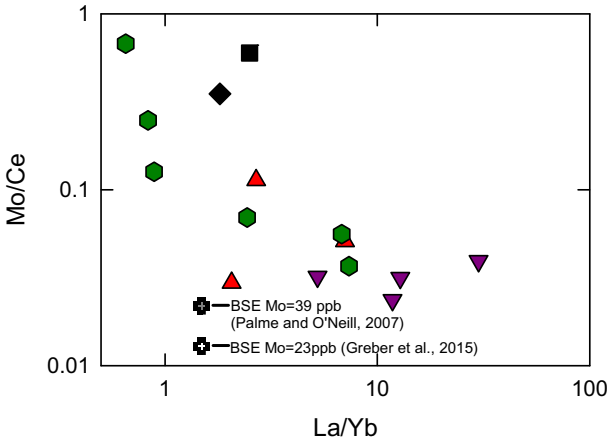

Fig. 5. La/Yb versus Mo/Ce for ultramafic rocks. Data from Table 1 and Appendix Table A1. Symbols as in Fig. 1.

a curve defined by the Vitim suite in particular, but the trend is negative; the most LREE depleted samples have the highest Mo/Ce as if Mo is significantly less incompatible than Ce. This is consistent with the similar behaviour of Al (Fig. 4b) implying that concentrations of Mo are dominated by the degree of major melting as opposed to cryptic metasomatism in the lithospheric samples. In other words Mo appears to be behaving as a less incompatible element in lithospheric mantle samples than has been inferred from studies of basalts. The lithospheric mantle samples exhibit both enrichment and depletion in LREEs, as is common. Yet all samples show [Mo], Mo/Mg and Mo/Ce that is enriched relative to the previously considered BSE based on basaltic rocks alone (Fig. 5).

5.3. MORB is isotopically uniform relative to the mantle

The MORBs are from various oceans and ridges, represented by four normal (N-type) and six enriched (E-type) samples. The lack of Mo isotopic difference between E-MORBs and N-MORBs is illustrated in Fig. 6. There is a slight hint in the data that Mo in both N- and E-MORB types may be very slightly lighter if the La/Yb is higher. However, this is not resolved in the current study. Therefore, the degree of partial melting is not exerting a simple control on Mo isotopes. The average composition 0.00 $\pm$ 0.02‰ is slightly heavier than the average chondrite composition of -0.14 ± 0.02‰ and the mean of the ultramafic xenoliths (-0.22 ± 0.06‰). Therefore, if there is any isotopic fractionation during melting it is small.

The Mo concentration of MORB has a mean of 0.48 $\pm$ 0.13 ppm (95% ci, Table 1), which is of similar order to the ultramafic xenoliths with a mean of 0.19 $\pm$ 0.07 ppm.

5.4. OIBs are variably fractionated isotopically

It is generally thought that MORBs are derived from the depleted upper mantle, whereas OIBs might originate from partial melting of plumes from the lower mantle (Allègre, 1982; Hofmann and White, 1982) and/or of relatively incompatible element enriched components in the heterogeneous upper mantle (Halliday et al., 1990, 1992; Fitton, 2007).

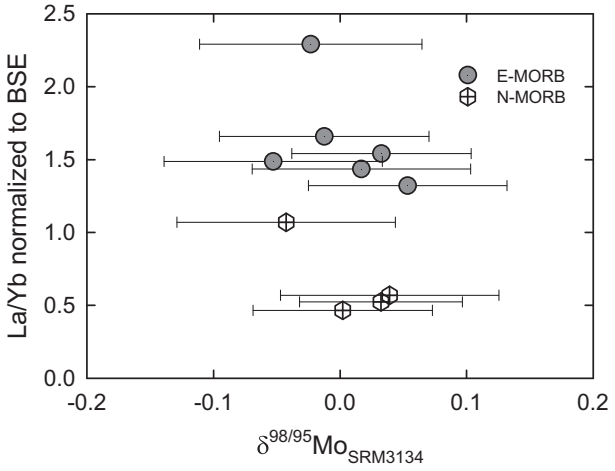

Fig. 6. $\delta^{98/95}$Mo values versus La/Yb ratios (normalized to BSE) for MORBs. Data from Table 1 and Appendix Table A1. Symbols as in Fig. 2.

As discussed earlier, due to the consistency of Mo isotope composition between E-MORBs and N-MORBs, Mo isotopic fractionation seems not to be simply controlled by the degree of partial melting. The situation for OIB is almost the opposite. There are differences both within OIB and between OIB and MORB. This could reflect a fundamental source difference but this would be hard to reconcile with the large $\delta^{98/95}$Mo variations between OIB samples from the same location, and even the same volcano (e.g. Etinde on the Cameroon Line). Twenty of these OIB samples have published Pb, Sr, and Nd isotope data, but no correlation is found between any of these parameters and Mo isotopes (Appendix Fig. 1a–c). Therefore, it seems most likely that source effects are minor and the Mo isotopic variations reflect a difference in magmatic processes associated with MORB and OIB production and differentiation.

The relationship between the $\delta^{98/95}$Mo variability and that of five incompatible trace element ratios in OIB is shown in Fig. 7. There are clear relationships that imply this is a source melting effect produced at small degrees of partial melting. For example Ce/Pb and Mo/Ce are thought to be uniform in OIB and MORB (Hofmann et al., 1986; Sims et al., 1990), yet these ratios seem to be fractionated in the samples with lower $\delta^{98/95}$Mo (Fig. 7a and d). There is a tendency for more LREE enriched basaltic samples to have slightly lower $\delta^{98/95}$Mo (Fig. 7e), providing evidence that either source enrichment or small degrees of partial melting or both are accompanied by Mo isotope fractionation. This is not a well defined correlation. A positive correlation (with $R^2 > 0.5$) is found however between both Mo/Pr and Mo/Ce and $\delta^{98/95}$Mo (Fig. 7c and d). Sample C152 from the Cameroon Line, has a particularly high Mo abundance and plots slightly above the other data. The most incompatible trace element enriched magmas (e.g. nephelinites) have the lowest Mo/Ce and Mo/Pr together with the lightest Mo. In particular, the Mo/Pr ratio of nephelinite C20 is much lower than all other samples and has the most negative $\delta^{98/95}$Mo (Figs. 2 and 7) implying that at small degrees of partial melting some phases partially retain isotopically heavy Mo. This is consistent with the negative trend of $\delta^{98/95}$Mo with La/Yb (Fig. 7e).

Molybdenum is chalcophile so one possible isotopically heavy phase might be a sulphide, although this has yet to be verified. The Mo/Ce ratio of basalt would then reflect buffering by a coexisting sulphide liquid during low degree partial melting. Leaching experiments from basalts indeed appear to confirm that sulphide is isotopically heavy relative to coexisting silicates (Voegelin et al., 2012). The fact that the Mo/Ce ratios of ultramafic xenoliths are systematically higher than in nearly all basaltic rocks (Fig. 8) is also might be explained by residual sulphides. However, this has yet to be evaluated with detailed studies of Mo distributions in ultramafic rocks.

The Ce/Pb ratios can be used to evaluate whether sulphides or sulphide liquids are the phases retaining isotopi-

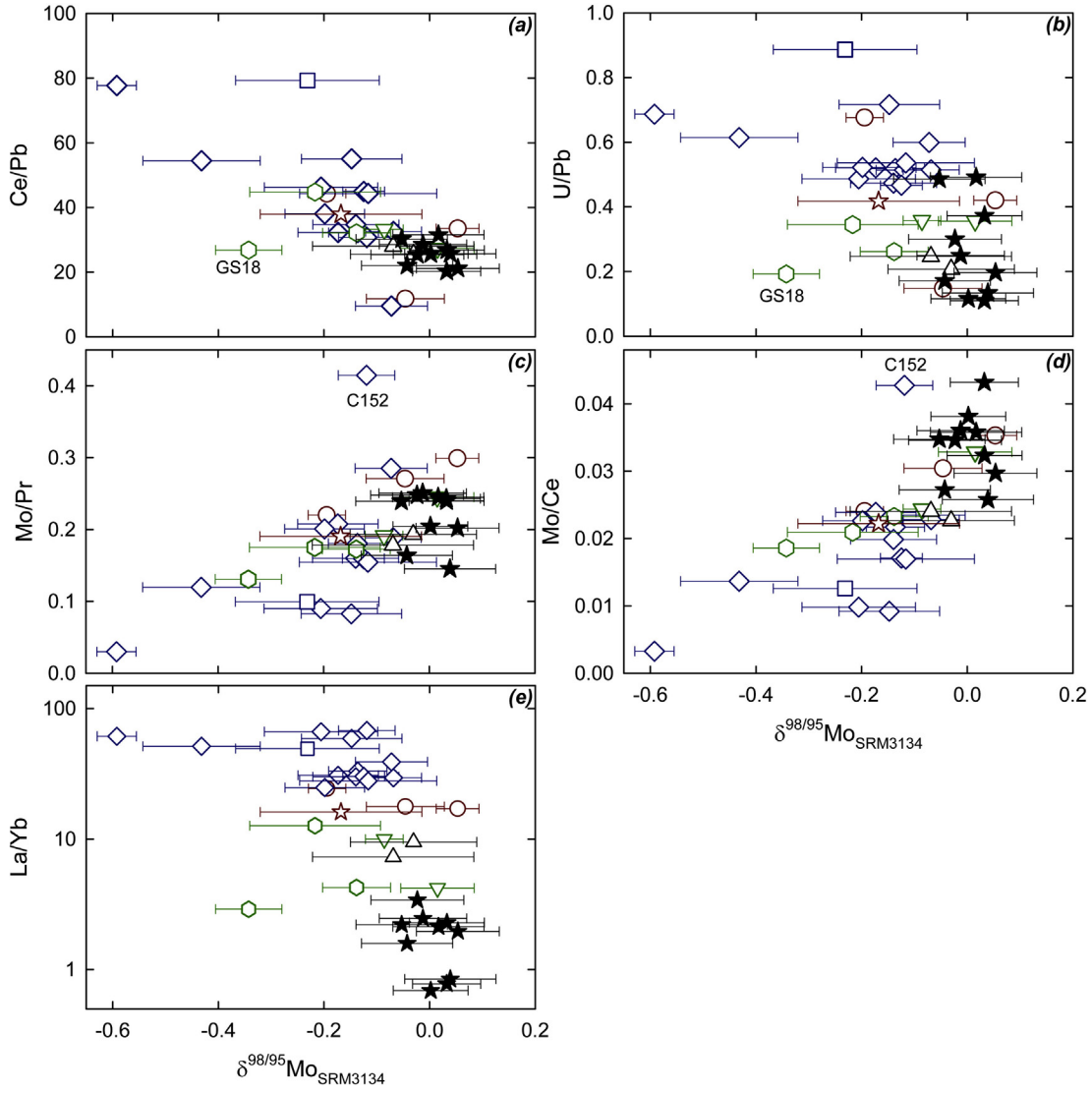

Fig. 7. (a) Ce/Pb, (b) U/Pb, (c) Mo/Pr, (d) Mo/Ce, and (e) La/Yb against $\delta^{98/95}$Mo values for OIBs and MORBs. Data from Table 1 and Appendix Table A1. Symbols as in Fig. 2.

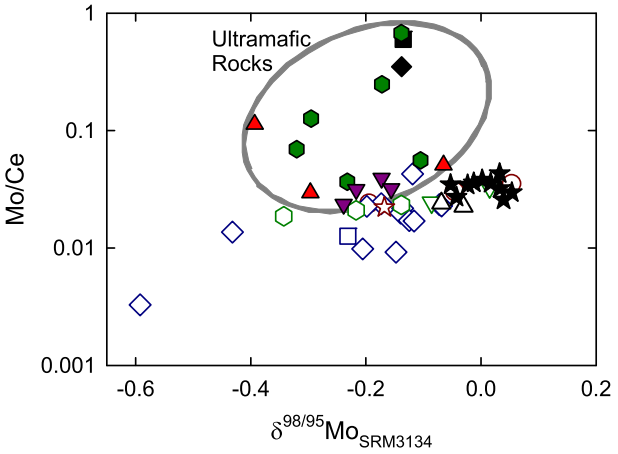

Fig. 8. $\delta^{98/95}$Mo versus Mo/Ce values for ultramafic xenoliths, OIBs and MORBs. Data from Table 1 and Appendix Table A1. Symbols as in Figs. 1 and 2.

cally heavy Mo in basalts. Uranium is well known to be more incompatible than Pb during mantle melting (Newsom et al., 1986), whereas Ce/Pb ratios are relatively uniform (Hofmann et al., 1986). Meijer et al. (1990) proposed that sulphide is likely to fractionate both U/Pb and Ce/Pb in ultramafic xenoliths. According to their calculation, all of the Pb in the mantle xenoliths they studied could be accounted for by just 0.15 wt.% of sulphide. Halliday et al. (1995) found fractionation in Ce/Pb and a positive correlation with U/Pb in highly incompatible element enriched magmas such as nephelinites. This observation was explained by small degree partial melting in the presence of residual sulphide (Halliday et al., 1995). The more enriched intraplate magmas studied here are from the same sample suite from the Cameroon Line and Trinidade (Halliday et al., 1988, 1990, 1992). Sims and DePaolo (1997) also showed from their global Pb and Ce data, that sulphide strongly influences the partitioning of Pb either

during shallow fractionation or as a mantle residue. More recently, Hart and Gaetani (2006) have proposed that sulphide fractionation during mantle melting might resolve the "Third Pb Paradox". This paradox is based on the relatively uniform Ce/Pb ratio in MORBs and OIBs over a wide range of absolute concentration, which should define the element ratio of the mantle but defines a Pb budget that is distinct from the well-established bulk silicate earth value inferred from Pb isotopes (Hofmann et al., 1986). Sims and DePaolo (1997) argued that Ce/Pb fractionation is widespread in sub-sets of global data, which indicates Pb is more compatible than Ce. They also suggested a role for sulphide in controlling the partitioning of Pb. Hofmann (2007) proposed that Nd is a slightly better surrogate for Pb than is Ce, but the Nd/Pb ratio of OIBs and N-MORBs are still higher than the bulk silicate earth (Hart and Gaetani, 2006). The role of sulphide in fractionating Pb has been confirmed by studies of inclusions in MORB, which have been shown to be exceedingly unradiogenic in their Pb isotopic composition (Burton et al., 2012; Warren and Shirey, 2012) and to represent a potentially important reservoir in solving the first Lead Paradox as well.

It can be seen in Fig. 7a and b that $\delta^{98/95}$Mo correlates inversely with both Ce/Pb and U/Pb (with $R^2 = 0.5$ and 0.4, respectively), providing evidence of fractionation by a similar process. The only sample plotting off the correlation is GS18, which is our most depleted Iceland sample. The La abundance of GS18 is less than 10 times primitive mantle and similar to MORB. Note that although all samples are petrographically fresh, samples with Ba/Rb less than 5 or more than 20 have been excluded, because this ratio has been shown to be especially sensitive to secondary alteration (Hofmann and White, 1983), which might affect Pb and Mo contents because they are potentially mobile during alteration. On this basis, 5 of the samples (AZP5, TD2, TD5, SNB19, and ST38) are excluded from further discussion.

Molybdenum is likely to be preferentially transported relative to rare earth elements such as Pr in high temperature fluids, fumaroles and volcanic aerosols (Dunn and Sen, 1994). Therefore, the correlations between Mo isotopes and Mo/Pr or Mo/Ce might in principle reflect loss of Mo by volcanic degassing as is found for Te and Re in subaerial basalts (Yi et al., 2000). However, when the Mo/Pr ratios of all OIBs, MORBs and Iceland samples are plotted against their Pr content in Fig. 9, there is no systematic difference between subaerial (Azores, Cameroon Line, Madeira, and Iceland) and submarine samples (Galapagos, Loihi and MORBs). Thus the relatively low Mo/Pr ratios of the Trinidade and a few of the Cameroon Line samples relate to these being incompatible element enriched nephelinites rather than being subaerial volcanic rocks. The scatter in Mo/Pr ratio for a given Pr concentration might itself be due to sulphide fractionation as mentioned by Newsom et al. (1986). They claimed that a sulphide fraction on the order of 0.1 wt.% would be sufficient to explain the observed Mo/Pr scatter in basalts.

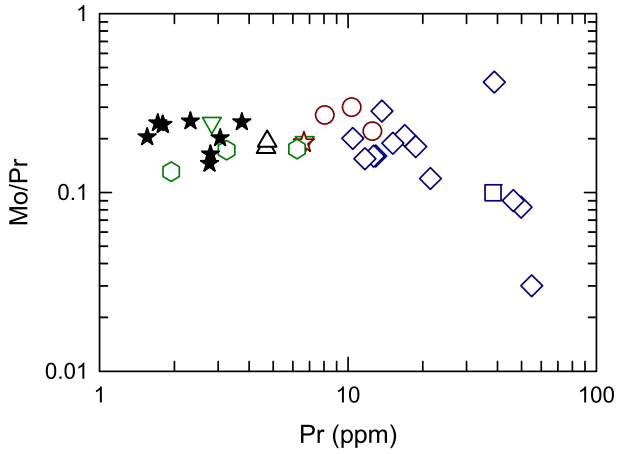

Fig. 9. Mo/Pr plotted against Pr content for OIBs and MORBs. Data from Table 1 and Appendix Table A1. Symbols as in Fig. 2.

5.5. Silicate–sulphide fractionation of molybdenum in the mantle

How sulphide fractionates chalcophile elements has been discussed by Yi et al. (2000) who argued that sulphide liquids would affect platinum group elements and Te even if they are not present in large quantities (Greenland and Aruscavage, 1986; Rehkamper et al., 1999). Based on experimental data, the sulphur contents at sulphide saturation is affected by pressure, temperature, melt composition, and oxygen fugacity (Mavrogenes and O'Neill, 1999; Liu et al., 2007). Melts might reach sulphide saturation during cooling, crystallization, or as new melts are added (Mavrogenes and O'Neill, 1999; Liu et al., 2007). Once sulphur solubility in silicate melts is exceeded immiscible sulphide will form and its removal will fractionate and deplete chalcophile elements (Yi et al., 2000).

Sulphide liquids could not only coexist with silicate melt but also be much denser, leading to their segregation if their size is sufficient (Czamanske and Moore, 1977). With their modelling, Hart and Gaetani (2006) suggested that sulphide melts might be likely to aggregate or pond at depth near the sulphide solidus because of their greater density relative to silicate melt; this strips Pb and potentially Mo from silicate liquids and solids.

Although Mo is not highly compatible in sulphides at upper mantle condition, it still prefers a monosulphide solid solution over sulphide liquid in silicate melts (Li and Audetat, 2012). While the partition coefficient of Mo between sulphide and silicate melt changes as a function of sulphur and oxygen fugacity (Lodders and Palme, 1991; Li and Audetat, 2012), this would not only influence the Mo abundance but also fractionate the Mo isotope composition between sulphides and silicate melts. This might explain why the Mo content and Mo/Ce values in ultramafic samples are not as well correlated with their $\delta^{98/95}$Mo values as they are in OIB samples (Fig. 8). With different sulphur and oxygen fugacity, the partition coefficient of Mo between sulphide and silicate melt changes over two orders of magnitude (Lodders and Palme, 1991; Li and Audetat, 2012), which might cause Mo/Ce heterogeneity in the mantle.

5.6. The concentrations and isotopic compositions of molybdenum in the mantle and bulk silicate Earth

If Mo is not as incompatible as was deduced from Mo/Ce in basalts and is being selectively retained in some way, a revised estimate of the BSE concentrations may be required. The Mo abundance of 39 ppb (Palme and O'Neill, 2007) for the primitive mantle and 25 ppb for the depleted mantle (Salters and Stracke, 2004) estimated from basalt data is more than an order of magnitude lower than the mean measured Mo concentration of the ultramafic xenoliths studied here (0.19 ± 0.18 ppm (95% ci)). Even the average reported Mo abundance (23 ppb) of modelled mantle source of komatiites are also much lower (Greber et al., 2015).

This discrepancy either reflects selective metasomatic enrichment of the subcontinental lithospheric mantle (as sampled by xenoliths), or a much higher [Mo] for the mantle than would be deduced from basalts because of selective retention of Mo in hidden phases such as segregated source sulphide liquids during melting (Hart and Gaetani, 2006). There are four lines of evidence that a selective Mo enrichment of the subcontinental lithosphere could be responsible.

1. The latest datasets for MORB glasses (Freymuth et al., 2015) display extremely well defined correlations between [Mo] and the concentrations of highly incompatible elements. This is hard to reconcile with some additional buffering process that is selectively retaining Mo in the mantle.
2. Data for Precambrian sediments demonstrate a strong correlation between selective Mo enrichment and heavy Mo isotopic compositions (Siebert et al., 2005), and if subducted may have added requisite anomalous Mo components to the subcontinental lithosphere over billions of years.
3. New data for arc volcanics (Freymuth et al., 2015; Konig et al., 2016) also provide evidence of selective Mo transfer via a fluid phase that is lost from the downgoing slab in the subduction environment. This fluid-mediated Mo component is also isotopically heavy.
4. The concentrations of Mo in the ultramafic xenoliths do not correlate well with those of other trace elements, while it seems that Mo abundance and Mo/Ce are lower in komatiites (Puchtel et al., 2004; Greber et al., 2015).

Therefore, there is evidence that the subcontinental lithosphere may not be representative of the asthenospheric mantle or the BSE.

To counter these arguments it is worth pointing out the apparent less incompatible behaviour of Mo in the ultramafic samples as indicated not just by the higher [Mo] (Fig. 3d) and higher Mo/Ce (Fig. 8) overall, but also the positive correlation between Al/Mg and Mo/Mg (Fig. 4b) and the striking negative correlation between Mo/Ce and La/Yb (Fig. 5). These features are more readily explained if Mo is not as incompatible as previously thought in the mantle represented by the ultramafic xenoliths. Finally, the average $\delta^{98/95}$Mo of the ultramafic xenoliths (-0.22 ± 0.06‰) is if anything lighter than MORB (0.00 ± 0.02‰), no different from the mean of OIB and Iceland (-0.14 ± 0.06‰ and -0.26 ± 0.12‰) and the average chondrite composition of -0.14 ± 0.02‰. There is no evidence that the ultramafic xenoliths are sampling a section of mantle that has been selectively enriched by isotopically heavy components from a subducting slab.

In the following therefore we consider the implications of the alternative – that the xenoliths do in fact reflect a higher [Mo] for the BSE than would otherwise be deduced, caused by selective retention of Mo during melting. There are very few published Mo concentration data for other ultramafic rocks with which to compare our results. Molybdenum concentrations (without REE data) were reported for a range of rock types by Kuroda and Sandell (1954). Limited data for komatiites are also available and these display a range from basaltic Mo/Ce to higher values (0.01–0.19) (Sims et al., 1990; Puchtel et al., 2004; Greber et al., 2015). Some of them could be affected by alteration and/or crustal contamination. Data are available for anomalously enriched assemblages (MARID-like rocks) in the suboceanic mantle (Gregoire et al., 2000). These four samples have highly variable Mo/Ce ranging between 0.02 and 0.16 consistent with the higher levels of Mo enrichment reported here Therefore, the available data are consistent with but do not verify a Mo/Ce and Mo concentration of the depleted mantle that is significantly higher than previously estimated. DTS-1, the most depleted ultramafic sample studied here, has one of the highest Mo/Ce ratios (~0.6). As previously pointed out, this may not be a reliable representative of the mantle.

If Mo is being partially retained during mantle melting and ultramafic samples have higher Mo/Ce ratio than basaltic mantle-derived samples (Fig. 8), one way of estimating a more reliable mantle Mo concentration might be based on the average Mo/Ce of our ultramafic samples and literature data for ultramafic rocks (Gregoire et al., 2000; Puchtel et al., 2004; Greber et al., 2015). This is 0.21, or an order of magnitude higher than previously reported values of 0.033 for the depleted mantle (Salters and Stracke, 2004) and 0.027 for the Primitive Mantle or BSE (Palme and O'Neill, 2007). The average Mo/Ce of our ultramafic samples is ~0.09, which is roughly 3 times higher than previously reported values. Using these estimates, the mantle is the major (>80%) repository for Mo in the silicate Earth.

The mean $\delta^{98/95}$Mo for ultramafic xenoliths of -0.22 ± 0.06‰ and chondrites (-0.14 ± 0.02‰) provides evidence that the BSE is close to chondritic given that this is dominated by the mantle composition. The $\delta^{98/95}$Mo and revised Mo concentration of the BSE assuming the depleted mantle is represented by the average ultramafic xenolith localities (and bearing in mind the uncertainty as to whether they are really representative of the upper mantle), and the oceanic (MORB average) and continental crust are given in Table 2. The Mo content of continental crust is as recommended previously (Rudnick and Gao, 2003), and the average continental crust $\delta^{98/95}$Mo is estimated to be in the range of 0.05–0.15‰ (Voegelin et al., 2014). The $\delta^{98/95}$Mo value thereby calculated for the BSE (-0.21 ± 0.06‰,

Table 2
Estimates of Mo content and $\delta^{98/95}$Mo value of the BSE.

	Mo abundance (ppb)	$\delta^{98/95}Mo_{SRM3134}$ (‰)
Continental Crust	800[a]	0.05–0.15[b]
Oceanic Crust	480	0.00 ± 0.02
Mantle	109(−177)	-0.22 ± 0.06
Bulk Silicate Earth	113(−180)	-0.21 ± 0.06

[a] Rudnick and Gao (2003)
[b] Voegelin et al. (2014), re-normalized to NIST SRM 3134.

Table 2) is similar to that of chondrites (-0.14 ± 0.02‰) and provides evidence that it may be lighter. It has been argued that the Mo isotopic composition of the BSE is between chondritic and 0 (that is, heavier) due to fractionation as a result of core formation (Burkhardt et al., 2014), in a similar fashion to that argued for Si (Georg et al., 2007; Armytage et al., 2011). It has now been shown using double spiking that Cr is not isotopically heavy in the BSE relative to chondrites (Bonnand et al., 2016). Our estimate of the BSE (Table 2, -0.21 ± 0.06‰) provides no evidence that Mo in the BSE is heavier than that in chondrites. Based on the latest experimental results, Hin et al. (2013) conclude that there is equilibrium fractionation of Mo isotopes between liquid metal and liquid silicate, but this fractionation is temperature dependent. There are three possible explanations for this apparent discrepancy:

1. These experiments did not include sulphur/sulphur-rich liquids under any experimental conditions, despite the fact that it has been shown that the partition coefficient of Mo between core-forming metallic and sulphur-rich liquids and silicate melt changes as a function of sulphur and oxygen fugacity (Lodders and Palme, 1991; Li and Audetat, 2012; Wade et al., 2012). Wade et al. (2012) showed that during metal–silicate partitioning, there is an exchange between oxidised Mo in the silicate and reduced Mo in the metal. In order to explain the BSE value determined here, heavy Mo isotopes would have to prefer the reducing conditions in the metal phase or sulphur-rich liquids, leaving the silicate enriched in light Mo. Partitioning of heavy Mo into sulphur-rich liquids would be consistent with our observations of mantle melting behaviour.
2. Given the uncertainties, it is also possible that the BSE and chondrites are close to identical (Greber et al., 2015 and this study) in which case it implies extremely high temperatures of core formation. As an example, according to the equation proposed by Hin et al. (2013), assuming the BSE and chondrites differ by <0.01‰ based on the mean of ordinary and CI chondrites and the estimated BSE Mo isotope composition, the temperature of core formation is calculated to be far above 3000 K. This would imply that Mo last equilibrated between metal and silicate at exceedingly high temperatures, such as those associated with the Moon forming Giant Impact (Cameron, 2000; Canup, 2004).
3. A lack of isotopic fractionation could also reflect addition of moderately siderophile elements to the BSE after core formation. O'Neill (1991) proposed that prior to the Giant Impact the Earth was highly reduced such that moderately siderophile elements were stripped into core forming metallic liquids. O'Neill proposed that Theia, the impacting planet, was highly oxidised and that the Fe and other moderately siderophile element abundances of the BSE were established at that point by the addition of broadly chondritic material. Only the highly siderophile elements were fractionated by further core formation.

Distinguishing between these possibilities will require a more precise determination of the Mo isotopic composition of the BSE. However, one can already surmise that the level of likeliness of each of these is different. If it is more negative than chondritic then the most likely explanation is fractionation by a sulphur-rich liquid (explanation 1 above). If it is almost identical the more likely explanation is high temperature core formation (2 above). If the BSE is exactly chondritic then the best explanation is perhaps the O'Neill (1991) model of an oxidised Theia (3 above). However, this model is inconsistent with the non-chondritic W isotopic composition of the BSE (Kleine et al., 2002; Schoenberg et al., 2002; Yin et al., 2002b) unless the Moon formed earlier than currently estimated. There is also one piece of evidence that suggests explanation 1 is less likely. The higher Mo abundance for the BSE suggested as a possible explanation for the xenolith data changes the constraints that exist on core formation. The prior high degree of depletion of Mo relative to Ni, W and Co was hard to explain without removal in late core forming sulphide liquids (Wade et al., 2012). The alternative estimate for the BSE based on ultramafic xenoliths is shown in Fig. 10. It can be seen that if this value is correct, Mo is now no more depleted than these other moderately siderophile elements and requires no special late removal mechanisms. If this is true, there is no evidence from Mo that the later stages of accretion were particularly sulphur or sulphide rich.

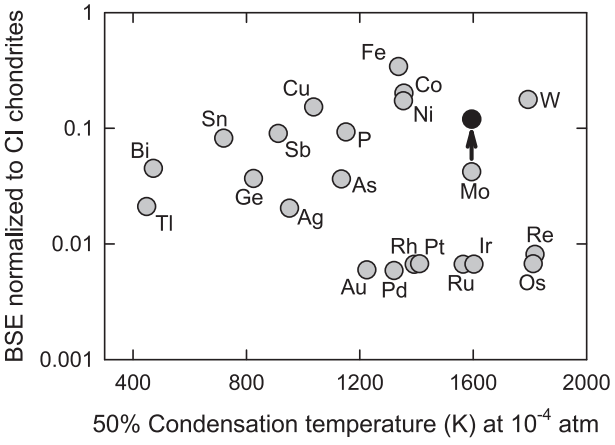

Fig. 10. Abundances of siderophile elements in the bulk silicate earth (normalized to CI chondrites) versus condensation temperatures. Data from Table 2 and Palme and O'Neill (2007).

Table A1
Major, trace element concentration, and radiogenic isotopes composition of terrestrial samples. For the data below, all of the major element concentration, radiogenic isotopes composition, and some of the trace element concentration are from literature (*in italic*), and the references have also been listed. The major element concentration of Tariat and Vitim samples were analyzed by XRF. The trace element concentration of those samples never measured before were analyzed by Agilent (Ultramafic Rocks) and Element (MORBs and OIBs) ICP-MS. Accuracy of major trace element concentration measurements is ±5%.

Sample	Locality	MgO (%)	Al_2O_3 (%)	La (ppm)	Ce (ppm)	Pr (ppm)	Yb (ppm)	Pb (ppm)	U (ppm)	$^{87}Sr/^{86}Sr$	$^{143}Nd/^{144}Nd$	$^{206}Pb/^{204}Pb$	Reference
Ultramafic rocks													
DTS-1	Twin Sisters, Washington	*49.6*	*0.19*	*0.03*	*0.05*		*0.01*						A; G
PCC-1	Cazadero Complex, California	*43.4*	*0.68*	*0.04*	*0.06*		*0.02*						A; G
KH96-8	Kilbourne Hole	*38.1*	*3.06*	*0.39*	*0.79*		*0.14*						F
KH03-10	Kilbourne Hole	*40.4*	*3.23*	*0.70*	*1.69*		*0.34*						F
KH03-16	Kilbourne Hole	*42.9*	*1.13*	*0.39*	*0.79*		*0.06*						F
ST0802	Tariat, Mongolia	37.3	4.06	0.38	1.15		0.45						
ST0803	Tariat, Mongolia	39.3	3.17	0.35	0.95		0.40						
ST0804	Tariat, Mongolia	38.9	3.08	2.57	5.19		0.38						
ST0805	Tariat, Mongolia	39.0	3.57	2.84	5.72		0.39						
ST0807	Tariat, Mongolia	39.6	2.98	0.97	1.87		0.40						
ST0809	Tariat, Mongolia	41.0	2.45	0.19	0.59		0.29						
PQ0902	Vitim, Siberia	41.2	1.75	2.75	3.42		0.09						
PQ0903	Vitim, Siberia	21.5	8.47	6.33	12.50		1.21						
PQ0910	Vitim, Siberia	38.5	2.97	2.24	4.79		0.17						
L-2-3	Vitim, Siberia	42.7	1.82	0.28	0.73		0.16						
Mid-ocean ridge basalts (MORB)													
MD34 D6	Southwest Indian Ridge			8.6	20.8	3.1	4.4	0.98	0.19				
45N	Mid-Atlantic Ridge			5.8	13.3	1.8	2.5	0.50	0.19				
ALV 518 3-1	Mid-Atlantic Ridge			5.0	11.7	1.7	2.3	0.37	0.18				
ALV 518 3-2	Mid-Atlantic Ridge			5.3	12.4	1.8	2.4	0.41	0.20				
ARP 1974 12-19	Mid-Atlantic Ridge			2.6	8.3	1.6	3.7	0.33	0.04				
CY82 18-01	East Pacific Rise			5.6	16.8	2.8	3.6	0.76	0.13				
DR 7-1	East Pacific Rise			11.2	26.8	3.7	3.3	1.06	0.32				
R82-1	East Pacific Rise			*1.6*	*5.4*	*1.0*	*2.1*	*0.26*	*0.03*				I
R93-7	East Pacific Rise			*6.2*	*16.2*	*2.3*	*2.5*	*0.57*	*0.14*				I
Searise 2 DR07	East Pacific Rise			4.8	15.6	2.8	5.6	0.61	0.08				
Plume-ridge interacting basalts													
CX19	Iceland			9.2	24.1	3.2	2.2	0.75	0.20	*0.70335*	*0.513022*		E
GS18	Iceland			5.6	13.7	1.9	1.9	0.51	0.10	*0.70315*	*0.513055*		E
SNB19	Iceland			*24.7*	*52.4*	*6.6*	*1.9*	*1.33*	*0.47*	*0.70332*	*0.513058*		H
SNB40	Iceland			23.4	52.1	6.2	1.8	1.17	0.40				
ST38	Iceland			12.7	29.9	3.8	2.2	0.82	0.22	*0.70338*	*0.513036*		E
Ocean island basalts (OIB) and continental intraplate basalts													
BCR-2	Columbia River, Oregon			*25*	*53*	*6.8*	*3.5*	*11*	*1.69*				J
BHVO-2	Halemaumau, Hawaii			*15*	*38*	*5.09*	*2*	*1.39*	*0.38*				K

AZF1	Azores	58.3	115	12.6	2.4	2.59	1.75	*0.70338*	*0.512969*	*19.282*	C
AZFY3	Azores	32.9	71.8	8.1	1.9	6.09	0.90	*0.70389*	*0.512878*	*18.637*	C
AZP5	Azores	15.5	33.6	4.2	1.3	1.06	0.29	*0.70370*	*0.512911*	*19.432*	C
AZP6	Azores	38.4	87.7	10.3	2.2	2.62	1.10	*0.70344*	*0.512946*	*19.464*	C
C1	Cameroon Line (Mt Cameroon)	72.3	147	16.9	2.3	4.56	2.38	*0.70333*	*0.512783*	*20.361*	D
C20	Cameroon Line (Etinde)	263	504	54.9	4.3	6.48	4.45				
C22	Cameroon Line (Etinde)	223	448	49.8	3.8	8.14	5.83				
C25	Cameroon Line (Mt Cameroon)	77.4	156	18.8	2.3	4.84	2.51	*0.70335*	*0.512777*	*20.354*	B
C30	Cameroon Line (Mt Cameroon)	51.3	104	12.9	1.7	3.00	1.42				
C51	Cameroon Line (Manengouba)	44.9	92.8	10.5	1.8	2.44	1.27	*0.70308*	*0.512929*	*19.920*	B
C72	Cameroon Line (Manengouba)	58.1	118	12.7	1.9	2.63	1.23	*0.70303*	*0.512867*	*20.182*	B
C128	Cameroon Line (Etinde)	226	425	46.3	3.4	9.18	4.47	*0.70341*	*0.512788*	*20.522*	D
C150	Cameroon Line (Etinde)	87.8	188	21.5	1.7	3.46	2.12	*0.70337*	*0.512800*	*20.289*	B
C152	Cameroon Line (Etinde)	212	377	38.8	3.1	12.3	6.30	*0.70331*	*0.512804*	*20.489*	B
C154	Cameroon Line (Etinde)	141	167	13.7	3.6	17.5	10.5	*0.70333*	*0.512835*	*20.522*	B
C192	Cameroon Line (Mt Cameroon)	61.4	125	15.2	2.1	3.85	1.98				
FP23	Cameroon Line (Bioko)	52.1	107	11.7	1.9	2.41	1.29	*0.70323*	*0.512843*	*20.298*	B
PL02 25-1	Galapagos	22.4	52.4	6.7	2.2	1.58	0.56				
PL02 30-1	Galapagos	9.6	21.1	2.8	2.3	0.77	0.27				
D4-6	Loihi	14.1	34.7	4.7	1.9	1.24	0.31				
D5-1	Loihi	16.9	40.3	4.7	1.8	1.58	0.33				
M40	Madeira	26.3	57.0	6.6	1.6	1.50	0.63	*0.70278*	*0.513113*	*19.143*	C
TD2	Trinidade	189	381	40.4	3.6	5.38	9.98				
TD4	Trinidade	168	303	38.4	3.4	3.83	3.39	*0.70380*	*0.512772*	*19.143*	C
TD5	Trinidade	115	253	31.3	2.9	4.37	2.81	*0.70384*	*0.512799*	*19.152*	C

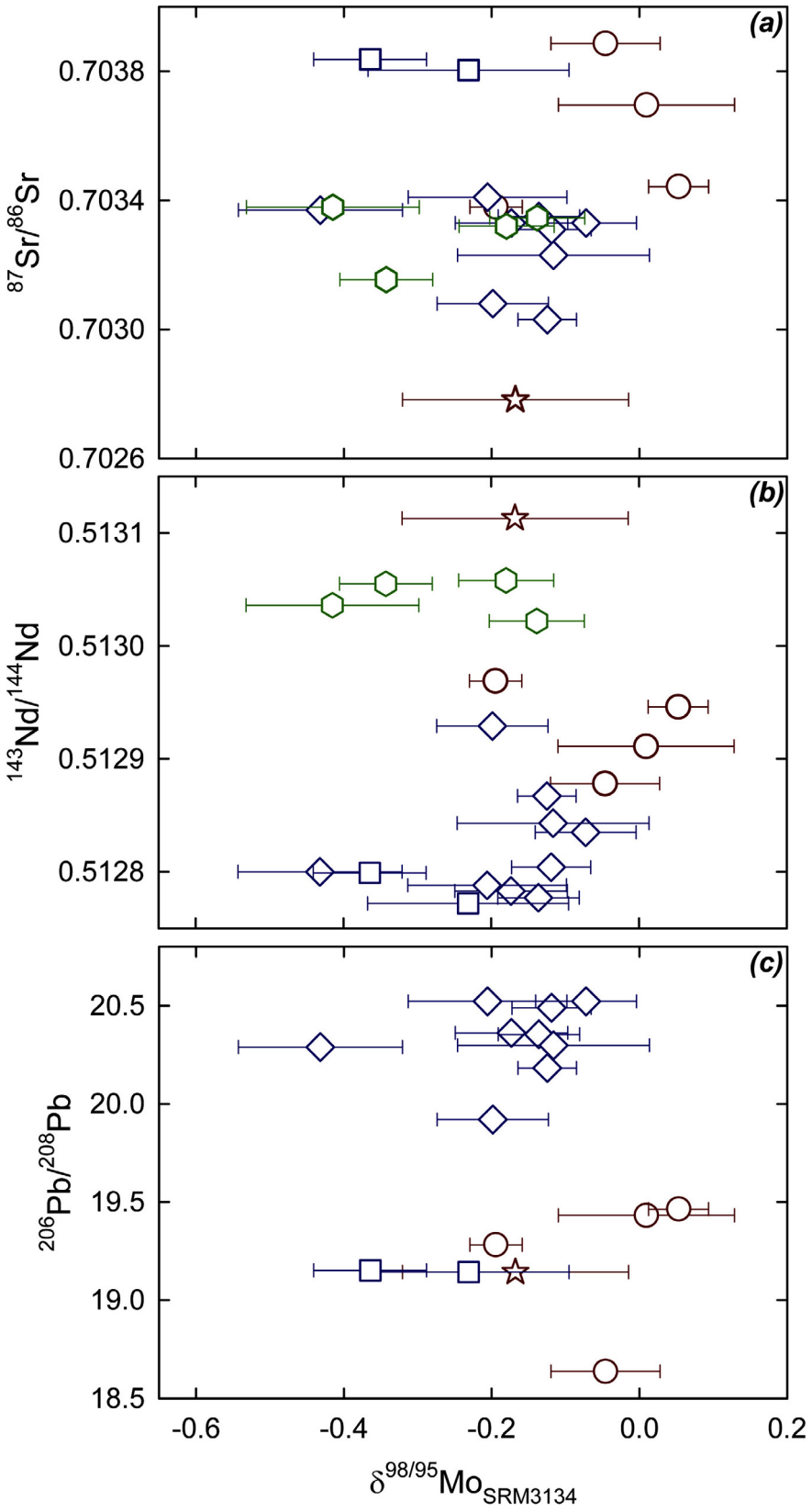

Fig. A1. Radiogenic (a) Sr, (b) Nd, and (c) Pb isotopes composition plotted against $\delta^{98/95}$Mo values for OIBs. Data from Table 1 and Appendix Table A1. Symbols as in Fig. 2.

6. CONCLUSIONS

1. The Mo isotopic composition of CI and ordinary chondrites are quite uniform and similar to the average for ultramafic xenoliths. However, the latter are more variable in both Mo content and isotopic composition.
2. Both Mo content and isotopic composition are uniform within MORB and similar to ultramafic xenoliths, but vary significantly in OIBs even within a single locality.
3. From the relationships between $\delta^{98/95}$Mo and Ce/Pb, U/Pb, Mo/Ce, and Mo/Pr it is suggested that residual sulphide liquids present at small degrees of partial melting in OIB sources may incorporate heavier Mo isotopes.
4. If residual sulphide is a significant Mo repository it could affect the calculated Mo budget of the mantle based on basalt compositions.
5. The high Mo concentrations in ultramafic xenoliths might either reflect this more compatible behaviour of Mo, or enrichment of the subcontinental lithospheric mantle.
6. If ultramafic xenoliths provide a better estimate of the composition of the mantle Mo concentration, then its concentration in the BSE is provisionally estimated to be 3 times higher than previously assumed. On this basis there is no need for there to be late removal of sulphur-rich liquids to the core.
7. The isotope composition of the BSE is currently not well constrained, but within error is identical to chondrites, i.e. the bulk Earth. Further work is needed to better define the exact isotopic composition of the BSE and elucidate if this is residual to loss of S rich core forming liquids, the result of high temperature (>2500) core formation, or addition of moderately siderophile elements from an oxidised Moon-forming impactor. Currently the second of these would seem most likely.

ACKNOWLEDGEMENTS

We are deeply grateful to Caroline Smith, Sara Russell, and Deborah Cassey at the Natural History Museum in London for providing the meteorite samples. Nick Belshaw, Philip Holdship, Fatima Mokadem, Jane Barling, and Jie Yang are thanked for invaluable assistance in the lab. We are grateful to Yaoling Niu and to the late Barry Dawson for samples. ANH acknowledges very helpful discussion with Tim Elliott, Thorsten Kleine, Christoph Burkhardt and Remco Hin. This research was supported by grants to ANH from ERC (NEWISOTOPEGEOSCIENCE. Award number: 247422) and STFC (ST/G00272X/1). The research materials supporting this publication can be accessed by contacting Prof. A.N. Halliday: alex.halliday@earth.ox.ac.uk.

APPENDIX A

APPENDIX B. SUPPLEMENTARY DATA

Supplementary data associated with this article can be found, in the online version, at http://dx.doi.org/10.1016/j.gca.2016.11.023.

REFERENCES

Allègre C. J. (1982) Chemical geodynamics. *Tectonophysics* **81**, 109–132.

Armytage R. M. G., Georg R. B., Savage P. S., Williams H. M. and Halliday A. N. (2011) Silicon isotopes in meteorites and planetary core formation. *Geochim. Cosmochim. Acta* **75**, 3662–3676.

Becker H. and Walker R. J. (2003) Efficient mixing of the solar nebula from uniform Mo isotopic composition of meteorites. *Nature* **425**, 152–155.

Bodinier J. L., Vasseur G., Vernieres J., Dupuy C. and Fabries J. (1990) Mechanisms of mantle metasomatism – geochemical evidence from the lherz orogenic peridotite. *J. Petrol.* **31**, 597–628.

Bonnand P., Williams H. M., Parkinson I. J., Wood B. J. and Halliday A. N. (2016) Stable chromium isotopic composition of meteorites and metal–silicate experiments: implications for fractionation during core formation. *Earth Planet. Sci. Lett.* **435**, 14–21.

Burkhardt C., Hin R. C., Kleine T. and Bourdon B. (2014) Evidence for Mo isotope fractionation in the solar nebula and during planetary differentiation. *Earth Planet. Sci. Lett.* **391**, 201–211.

Burkhardt C., Kleine T., Oberli F., Pack A., Bourdon B. and Wieler R. (2011) Molybdenum isotope anomalies in meteorites: constraints on solar nebula evolution and origin of the Earth. *Earth Planet. Sci. Lett.* **312**, 390–400.

Burton K. W., Cenki-Tok B., Mokadem F., Harvey J., Gannoun A., Alard O. and Parkinson I. J. (2012) Unradiogenic lead in Earth's upper mantle. *Nat. Geosci.* **5**, 570–573.

Cameron A. G. (2000) Higher resolution simulations of the giant impact. In *Origin of the Earth and Moon* (ed. R. M. C. K. Righter). University of Arizona Press, Tucson, pp. 133–144.

Canup R. M. (2004) Simulations of a late lunar-forming impact. *Icarus* **168**, 433–456.

Czamanske G. K. and Moore J. G. (1977) Composition and phase chemistry of sulfide globules in basalt from the Mid-Atlantic Ridge rift valley near 37 N lat. *Geol. Soc. Am. Bull.* **88**, 587–599.

Dauphas N., Marty B. and Reisberg L. (2002) Inference on terrestrial genesis from molybdenum isotope systematics. *Geophys. Res. Lett.* **29**.

Dawson J. B. (2002) Metasomatism and partial melting in upper-mantle peridotite xenoliths from the Lashaine volcano, northern Tanzania. *J. Petrol.* **43**, 1749–1777.

Dunn T. and Sen C. (1994) Mineral/matrix partition-coefficients for ortho-pyroxene, plagioclase, and olivine in basaltic to andesitic systems – a combined analytical and experimental-study. *Geochim. Cosmochim. Acta* **58**, 717–733.

Endress M., Zinner E. and Bischoff A. (1996) Early aqueous activity on primitive meteorite parent bodies. *Nature* **379**, 701–703.

Fitton J. G. (2007) The OIB paradox. In *Plates, Plumes and Planetary Processes* (eds. G. R. Foulger and D. M. Jurdy). pp. 387–409.

Flanagan F. J. (1967) U.S. Geological Survey silicate rock standards. *Geochim. Cosmochim. Acta* **31**, 289-&.

Freymuth H., Vils F., Willbold M., Taylor R. N. and Elliott T. (2015) Molybdenum mobility and isotopic fractionation during subduction at the Mariana arc. *Earth Planet. Sci. Lett.* **432**, 176–186.

Galer S. J. G. and O'Nions R. K. (1986) Magmagenesis and the mapping of chemical and isotopic variations in the mantle. *Chem. Geol.* **56**, 45–61.

Gannoun A., Burton K. W., Parkinson I. J., Alard O., Schiano P. and Thomas L. E. (2007) The scale and origin of the osmium

isotope variations in mid-ocean ridge basalts. *Earth Planet. Sci. Lett.* **259**, 541–556.
Georg R. B., Halliday A. N., Schauble E. A. and Reynolds B. C. (2007) Silicon in the Earth's core. *Nature* **447**, 1102–1106.
Greber N. D., Pettke T. and Nägler T. F. (2014) Magmatic-hydrothermal molybdenum isotope fractionation and its relevance to the igneous crustal signature. *Lithos* **190–191**, 104–110.
Greber N. D., Puchtel I. S., Nagler T. F. and Mezger K. (2015) Komatiites constrain molybdenum isotope composition of the Earth's mantle. *Earth Planet. Sci. Lett.* **421**, 129–138.
Greber N. D., Siebert C., Naegler T. F. and Pettke T. (2012) $d^{98/95}$Mo values and molybdenum concentration data for NIST SRM 610, 612 and 3134: towards a common protocol for reporting Mo data. *Geostand. Geoanal. Res.* **36**, 291–300.
Greenland L. P. and Aruscavage P. (1986) Volcanic emission of Se, Te, and As from Kilauea volcano, Hawaii. *J. Volcanol. Geotherm. Res.* **27**, 195–201.
Gregoire M., Lorand J. P., O'Reilly S. Y. and Cottin J. Y. (2000) Armalcolite-bearing, Ti-rich metasomatic assemblages in harzburgitic xenoliths from the Kerguelen Islands: implications for the oceanic mantle budget of high-field strength elements. *Geochim. Cosmochim. Acta* **64**, 673–694.
Halliday A. N., Davidson J. P., Holden P., Dewolf C., Lee D. C. and Fitton J. G. (1990) Trace-element fractionation in plumes and the origin of HIMU mantle beneath the Cameroon line. *Nature* **347**, 523–528.
Halliday A. N., Davies G. R., Lee D. C., Tommasini S., Paslick C. R., Fitton J. G. and James D. E. (1992) Lead isotope evidence for young trace element enrichment in the oceanic upper mantle. *Nature* **359**, 623–627.
Halliday A. N., Dickin A. P., Fallick A. E. and Fitton J. G. (1988) Mantle dynamics: a Nd, Sr, Pb and O isotopic study of the cameroon line volcanic chain. *J. Petrol.* **29**, 181–211.
Halliday A. N., Lee D. C., Tommasini S., Davies G. R., Paslick C. R., Fitton J. G. and James D. E. (1995) Incompatible trace elements in OIB and MORB and source enrichment in the sub-oceanic mantle. *Earth Planet. Sci. Lett.* **133**, 379–395.
Hannah J. L., Stein H. J., Wieser M. E., de Laeter J. R. and Varner M. D. (2007) Molybdenum isotope variations in molybdenite: vapor transport and Rayleigh fractionation of Mo. *Geology* **35**, 703–706.
Hardarson B. S. and Fitton J. G. (1997) Mechanisms of crustal accretion in Iceland. *Geology* **25**, 1043–1046.
Harris N., Hunt A., Parkinson I., Tindle A., Yondon M. and Hammond S. (2010) Tectonic implications of garnet-bearing mantle xenoliths exhumed by Quaternary magmatism in the Hangay dome, central Mongolia. *Contrib. Mineral. Petrol.* **160**, 67–81.
Hart S. R. and Gaetani G. A. (2006) Mantle Pb paradoxes: the sulfide solution. *Contrib. Mineral. Petrol.* **152**, 295–308.
Harvey J., Dale C. W., Gannoun A. and Burton K. W. (2011) Osmium mass balance in peridotite and the effects of mantle-derived sulphides on basalt petrogenesis. *Geochim. Cosmochim. Acta* **75**, 5574–5596.
Harvey J., Yoshikawa M., Hammond S. J. and Burton K. W. (2012) Deciphering the trace element characteristics in kilbourne hole peridotite xenoliths: melt–rock interaction and metasomatism beneath the Rio Grande Rift, SW USA. *J. Petrol.* **53**, 1709–1742.
Hin R. C., Burkhardt C., Schmidt M. W., Bourdon B. and Kleine T. (2013) Experimental evidence for Mo isotope fractionation between metal and silicate liquids. *Earth Planet. Sci. Lett.* **379**, 38–48.
Hofmann A. W. and White W. M. (1982) Mantle plumes from ancient oceanic-crust. *Earth Planet. Sci. Lett.* **57**, 421–436.
Hofmann A. W. and White W. M. (1983) Ba, Rb and Cs in the earths mantle. *Z. Naturfors. Sect. A-J. Phys. Sci.* **38**, 256–266.
Hofmann A. W. (2007) 2.03 – sampling mantle heterogeneity through oceanic basalts: isotopes and trace elements. In *Treatise on Geochemistry* (eds. H. D. Holland and K. K. Turekian). Pergamon, Oxford, pp. 1–44.
Hofmann A. W., Jochum K. P., Seufert M. and White W. M. (1986) Nb and Pb in oceanic basalts: new constraints on mantle evolution. *Earth Planet. Sci. Lett.* **79**, 33–45.
Ionov D. (2004) Chemical variations in peridotite xenoliths from Vitim, Siberia: inferences for REE and Hf behaviour in the garnet-facies upper mantle. *J. Petrol.* **45**, 343–367.
Ionov D. A. (2007) Compositional variations and heterogeneity in fertile lithospheric mantle: peridotite xenoliths in basalts from Tariat, Mongolia. *Contrib. Mineral. Petrol.* **154**, 455–477.
Ionov D. A., Ashchepkov I. and Jagoutz E. (2005) The provenance of fertile off-craton lithospheric mantle: Sr–Nd isotope and chemical composition of garnet and spinel peridotite xenoliths from Vitim, Siberia. *Chem. Geol.* **217**, 41–75.
Ionov D. A., Bodinier J. L., Mukasa S. B. and Zanetti A. (2002) Mechanisms and sources of mantle metasomatism: major and trace element compositions of peridotite xenoliths from Spitsbergen in the context of numerical modelling. *J. Petrol.* **43**, 2219–2259.
Kleine T., Munker C., Mezger K. and Palme H. (2002) Rapid accretion and early core formation on asteroids and the terrestrial planets from Hf–W chronometry. *Nature* **418**, 952–955.
Konig S., Wille M., Voegelin A. and Schoenberg R. (2016) Molybdenum isotope systematics in subduction zones. *Earth Planet. Sci. Lett.* **447**, 95–102.
Krot A. N., Keil K., Scott E. R. D., Goodrich C. A. and Weisberg M. K. (2007) 1.05 – Classification of meteorites. In *Treatise on Geochemistry* (eds. D. H. Heinrich and K. T. Karl). Pergamon, Oxford, pp. 1–52.
Kuroda P. K. and Sandell E. B. (1954) Geochemistry of molybdenum. *Geochim. Cosmochim. Acta* **6**, 35–63.
Lee D. C., Halliday A. N., Davies G. R., Essene E. J., Fitton J. G. and Temdjim R. (1996) Melt enrichment of shallow depleted mantle: a detailed petrological, trace element and isotopic study of Mantle-Derived xenoliths and megacrysts from the Cameroon line. *J. Petrol.* **37**, 415–441.
Li Y. and Audetat A. (2012) Partitioning of V, Mn Co, Ni, Cu, Zn, As, Mo, Ag, Sn, Sb, W, Au, Pb, and Bi between sulfide phases and hydrous basanite melt at upper mantle conditions. *Earth Planet. Sci. Lett.* **355**, 327–340.
Liang Y. H., Siebert C., Fitton J. G., Burton K. W. and Halliday A. N. (2013) Molybdenum isotope fractionation in the mantle. **77**, 1607.
Liu Y., Samaha N.-T. and Baker D. R. (2007) Sulfur concentration at sulfide saturation (SCSS) in magmatic silicate melts. *Geochim. Cosmochim. Acta* **71**, 1783–1799.
Lodders K. and Palme H. (1991) On the chalcophile character of molybdenum: determination of sulfide/silicate partition coefficients of Mo and W. *Earth Planet. Sci. Lett.* **103**, 311–324.
Mathur R., Brantley S., Anbar A., Munizaga F., Maksaev V., Newberry R., Vervoort J. and Hart G. (2010) Variation of Mo isotopes from molybdenite in high-temperature hydrothermal ore deposits. *Miner. Depos.* **45**, 43–50.
Mavrogenes J. A. and O'Neill H. S. C. (1999) The relative effects of pressure, temperature and oxygen fugacity on the solubility of sulfide in mafic magmas. *Geochim. Cosmochim. Acta* **63**, 1173–1180.
Meijer A., Kwon T. T. and Tilton G. R. (1990) U–Th–Pb partitioning behavior during partial melting in the upper mantle: implications for the origin of high Mu components

and the "Pb paradox". *J. Geophys. Res. Solid Earth Planets* **95**, 433–448.

Navon O. and Stolper E. (1987) Geochemical consequences of melt percolation – the upper mantle as a chromatographic column. *J. Geol.* **95**, 285–307.

Newsom H. E., White W. M., Jochum K. P. and Hofmann A. W. (1986) Siderophile and chalcophile element abundances in oceanic basalts, Pb isotope evolution and growth of the Earth's core. *Earth Planet. Sci. Lett.* **80**, 299–313.

Niu Y. L. and Batiza R. (1997) Trace element evidence from seamounts for recycled oceanic crust in the eastern Pacific mantle. *Earth Planet. Sci. Lett.* **148**, 471–483.

O'Neill H. S. (1991) The origin of the moon and the early history of the earth – a chemical-model. 2. The Earth. *Geochim. Cosmochim. Acta* **55**, 1159–1172.

Onyeagocha A. C. (1978) Twin Sisters dunite: petrology and mineral chemistry. *Geol. Soc. Am. Bull.* **89**, 1459–1474.

Palme H. and O'Neill H. S. C. (2007) 2.01 – Cosmochemical estimates of mantle composition. In *Treatise on Geochemistry* (eds. D. H. Heinrich and K. T. Karl). Pergamon, Oxford, pp. 1–38.

Prytulak J., Nielsen S. G. and Halliday A. N. (2011) Determination of precise and accurate V-51/V-50 isotope ratios by multi-collector ICP-MS, Part 2: isotopic composition of six reference materials plus the allende chondrite and verification tests. *Geostand. Geoanal. Res.* **35**, 307–318.

Puchtel I. S., Brandon A. D. and Humayun M. (2004) Precise Pt–Re–Os isotope systematics of the mantle from 2.7-Ga komatiites. *Earth Planet. Sci. Lett.* **224**, 157–174.

Rehkamper M., Halliday A. N., Fitton J. G., Lee D. C., Wieneke M. and Arndt N. T. (1999) Ir, Ru, Pt, and Pd in basalts and komatiites: new constraints for the geochemical behavior of the platinum-group elements in the mantle. *Geochim. Cosmochim. Acta* **63**, 3915–3934.

Rudnick R. L. and Gao S. (2003) 3.01 – Composition of the continental crust. In *Treatise on Geochemistry* (eds. D. H. Heinrich and K. T. Karl). Pergamon, Oxford, pp. 1–64.

Salters V. J. M. and Stracke A. (2004) Composition of the depleted mantle. *Geochem. Geophys. Geosyst.* **5**.

Schiano P., Birck J. L. and Allegre C. J. (1997) Osmium–strontium–neodymium–lead isotopic covariations in mid-ocean ridge basalt glasses and the heterogeneity of the upper mantle. *Earth Planet. Sci. Lett.* **150**, 363–379.

Schilling J. G., Meyer P. S. and Kingsley R. H. (1982) Evolution of the Iceland hotspot. *Nature* **296**, 313–320.

Schoenberg R., Kamber B. S., Collerson K. D. and Eugster O. (2002) New W-isotope evidence for rapid terrestrial accretion and very early core formation. *Geochim. Cosmochim. Acta* **66**, 3151–3160.

Siebert C., Kramers J. D., Meisel T., Morel P. and Nagler T. F. (2005) PGE, Re–Os, and Mo isotope systematics in Archean and early Proterozoic sedimentary systems as proxies for redox conditions of the early Earth. *Geochim. Cosmochim. Acta* **69**, 1787–1801.

Siebert C., Nagler T. F. and Kramers J. D. (2001) Determination of molybdenum isotope fractionation by double-spike multicollector inductively coupled plasma mass spectrometry. *Geochem. Geophys. Geosyst.* **2**, art. no. -2000GC000124.

Sims K. W. W. and DePaolo D. J. (1997) Inferences about mantle magma sources from incompatible element concentration ratios in oceanic basalts. *Geochim. Cosmochim. Acta* **61**, 765–784.

Sims K. W. W., Newsom H. E. and Gladney E. S. (1990) Chemical fractionation during formation of the Earth's core and continental crust: clues from As, Sb, W and Mo. In *Origin of the Earth* (eds. H. E. Newsom and J. H. Jones). Oxford University Press, Oxford, pp. 291–317.

Soustelle V., Tommasi A., Bodinier J. L., Garrido C. J. and Vauchez A. (2009) Deformation and reactive melt transport in the mantle lithosphere above a large-scale partial melting domain: the Ronda peridotite massif, Southern Spain. *J. Petrol.* **50**, 1235–1266.

Vasseur G., Vernieres J. and Bodinier J. L. (1991) Modelling of trace element transfer between mantle melt and heterogranular peridotite matrix. *J. Petrol.*, 41–54.

Voegelin A. R., Naegler T. F., Pettke T., Neubert N., Steinmann M., Pourret O. and Villa I. M. (2012) The impact of igneous bedrock weathering on the Mo isotopic composition of stream waters: natural samples and laboratory experiments. *Geochim. Cosmochim. Acta* **86**, 150–165.

Voegelin A. R., Pettke T., Greber N. D., von Niederhäusern B. and Nägler T. F. (2014) Magma differentiation fractionates Mo isotope ratios: evidence from the Kos Plateau Tuff (Aegean Arc). *Lithos* **190–191**, 440–448.

Wade J., Wood B. J. and Tuff J. (2012) Metal–silicate partitioning of Mo and W at high pressures and temperatures: evidence for late accretion of sulphur to the Earth. *Geochim. Cosmochim. Acta* **85**, 58–74.

Walter M. J. (2003) 2.08 – melt extraction and compositional variability in mantle lithosphere. In *Treatise on Geochemistry* (eds. H. D. Holland and K. K. Turekian). Pergamon, Oxford, pp. 363–394.

Wang K.-L., O'Reilly S. Y., Kovach V., Griffin W. L., Pearson N. J., Yarmolyuk V., Kuzmin M. I., Chieh C.-J., Shellnutt J. G. and Iizuka Y. (2013) Microcontinents among the accretionary complexes of the Central Asia Orogenic Belt: in situ Re–Os evidence. *J. Asian Earth Sci.* **62**, 37–50.

Warren J. M. and Shirey S. B. (2012) Lead and osmium isotopic constraints on the oceanic mantle from single abyssal peridotite sulfides. *Earth Planet. Sci. Lett.* **359–360**, 279–293.

Yang J., Siebert C., Barling J., Savage P., Liang Y. H. and Halliday A. N. (2015) Absence of molybdenum isotope fractionation during magmatic differentiation at Hekla volcano, Iceland. *Geochim. Cosmochim. Acta* **162**, 126–136.

Yi W., Halliday A. N., Alt J. C., Lee D. C., Rehkamper M., Garcia M. O. and Su Y. J. (2000) Cadmium, indium, tin, tellurium, and sulfur in oceanic basalts: implications for chalcophile element fractionation in the Earth. *J. Geophys. Res. Solid Earth* **105**, 18927–18948.

Yi W., Halliday A. N., Lee D. C. and Christensen J. N. (1995) Indium and tin in basalts, sulfides, and the mantle. *Geochim. Cosmochim. Acta* **59**, 5081–5090.

Yin Q. Z., Jacobsen S. B. and Yamashita K. (2002a) Diverse supernova sources of pre-solar material inferred from molybdenum isotopes in meteorites. *Nature* **415**, 881–883.

Yin Q. Z., Jacobsen S. B., Yamashita K., Blichert-Toft J., Telouk P. and Albarede F. (2002b) A short timescale for terrestrial planet formation from Hf–W chronometry of meteorites. *Nature* **418**, 949–952.

Associate editor: Nicolas Dauphas